



**HAL**  
open science

## Forecasting contrasting coastal and estuarine hydrodynamics with OPENCoastS

Anabela Oliveira, André B Fortunato, Marta Rodrigues, Alberto Azevedo, João Rogeiro, Samuel Bernardo, Laura Lavaud, X. Bertin, Alphonse Nahon, Gonçalo de Jesus, et al.

► **To cite this version:**

Anabela Oliveira, André B Fortunato, Marta Rodrigues, Alberto Azevedo, João Rogeiro, et al.. Forecasting contrasting coastal and estuarine hydrodynamics with OPENCoastS. *Environmental Modelling and Software*, 2021, 143, pp.105132. 10.1016/j.envsoft.2021.105132 . hal-03454644

**HAL Id: hal-03454644**

**<https://univ-rochelle.hal.science/hal-03454644v1>**

Submitted on 29 Nov 2021

**HAL** is a multi-disciplinary open access archive for the deposit and dissemination of scientific research documents, whether they are published or not. The documents may come from teaching and research institutions in France or abroad, or from public or private research centers.

L'archive ouverte pluridisciplinaire **HAL**, est destinée au dépôt et à la diffusion de documents scientifiques de niveau recherche, publiés ou non, émanant des établissements d'enseignement et de recherche français ou étrangers, des laboratoires publics ou privés.

# Forecasting contrasting coastal and estuarine hydrodynamics with OPENCoastS

A. Oliveira,<sup>1,\*</sup> A.B. Fortunato,<sup>1</sup> M. Rodrigues,<sup>1</sup> A. Azevedo,<sup>1</sup> J. Rogeiro,<sup>1</sup> S. Bernardo,<sup>2</sup> Laura Lavaud,<sup>3</sup> Xavier Bertin,<sup>3</sup> Alphonse Nahon,<sup>1</sup> Gonçalo de Jesus,<sup>1</sup> Miguel Rocha,<sup>1</sup> P. Lopes<sup>1</sup>

**1 - National Laboratory for Civil Engineering, Av. do Brasil, 101, 1700-066 Lisbon, Portugal**

**2- LIP, Av. Gama Pinto, n.2, piso 3. Complexo Interdisciplinar (3is) 1649-003 Lisboa**

**3 - UMR 7266 LIENSs, CNRS-La Rochelle Université, 2 rue Olympe de Gouges, 17000 La Rochelle, France.**

**\* Corresponding author**

**Submitted to Environmental Modeling & Software, April, 2021**

**Reviewed, July, 2021**

## Highlights

- Web platform to generate on-demand forecast systems for multiple circulation options
- Open source software at <https://opencoasts.ncg.ingrid.pt/>, using EOSC resources
- Forced by GFS, WRF or ARPEGE (atmosphere), CMEMS or FES2014 (ocean) and WW3 (waves)
- Data/model comparison with Copernicus Sentinel data and in-situ EMODnet field data

## Abstract

1 Robust and accurate coastal forecasts require models to represent the relevant  
2 processes, prediction computational tools and reliable computational resources.  
3 OPENCoastS is a free, open-source WebGIS platform to develop on-demand  
4 hydrodynamic forecast systems that started as a simple 2D engine.  
5 OPENCoastS provides a visualization and download interface with in-situ and  
6 Sentinel satellite data comparison. 2D tidal, 2D wave & current interaction and  
7 3D baroclinic flows are now included, forced by several atmospheric, oceanic  
8 and riverine forcings.  
9

10 Four applications demonstrate OPENCoastS' capacity. The prediction of the  
11 2020 typhoon season in Taiwan illustrates the use of the service using only  
12 large-scale public data. An application to the Bay of Biscay shows the  
13 importance of waves on extreme water levels during storms. A nearshore  
14 deployment in Figueira da Foz harbor assesses the impact of bathymetry on  
15 coupled wave and current circulation. 3D baroclinic circulation forecasts in  
16 Tagus estuary are validated by independent data.  
17

18 **Keywords:** SCHISM, Forecast systems, Unstructured grids, cross-scale, EOSC,  
19 Wave and currents modeling, Baroclinic modeling  
20

## 21 **Software availability**

22 Program title

23 OPENCoastS

24 Developers

25 João Rogeiro, Joana Teixeira, Pedro Lopes, Gonçalo de Jesus, Miguel  
26 Rocha, Alberto Azevedo, Marta Rodrigues, André Fortunato  
27

28 Contact address

29 [jrogeiro@lnec.pt](mailto:jrogeiro@lnec.pt)

30 Software Access

31 <https://opencoasts.ncg.ingrid.pt/>

32 Year first available

33 2018 (v1); 2021 (v2)

34 Software required

35 Browser: Firefox, Google Chrome  
36  
37  
38  
39  
40  
41  
42  
43  
44  
45  
46  
47  
48  
49  
50  
51  
52  
53  
54  
55  
56  
57  
58  
59  
60  
61  
62  
63  
64  
65

1 Program language  
2 Python & HTML+CSS+JavaScript  
3

4 Availability and cost

5 Access for usage: Open access upon registration (email required)  
6

7  
8 Access to source code: Free software with an Apache License Version 2.0  
9 available in: <https://gitlab.com/opencoasts/eosc-hub>  
10  
11

## 12 13 14 **1. Introduction** 15

16  
17 Coastal forecast systems provide predictions of environmental variables at time  
18 scales of a few days. Environmental variables include water levels, velocities,  
19 wave parameters, pollutant concentrations and sediment fluxes. These forecast  
20 systems have a wide range of applications in coastal and harbor management  
21 (Viegas et al., 2009; Bedri et al., 2014; Oliveira et al., 2015), civil protection  
22 (Breivik and Allen, 2008; Fortunato et al., 2017a; Ferrarin et al., 2019; Stokes et  
23 al., 2020), navigation (Orseau et al., 2021), military operations and recreation  
24 (e.g. windguru.cz, magicseaweed.com). Some of these forecast systems cover  
25 spatial scales from oceans and regional seas to coastal regions, using  
26 downscaling techniques over structured and unstructured grids (Trotta et al.,  
27 2016, 2021). They are developed and operated by research centers,  
28 meteorological and hydrographic organizations, harbor administrations and  
29 private companies.  
30

31  
32 In spite of the growing development of coastal forecast systems, their  
33 dissemination remains limited by their implementation and maintenance costs.  
34 These costs are mostly associated with very specialized human resources, with  
35 backgrounds in both numerical modeling and information technologies, and also  
36 with dedicated computational resources to guarantee a timely delivery of  
37 predictions.  
38

39  
40 However, several evolutions are paving the way for a drastic increase in the  
41 development and adoption of coastal forecast systems. First, higher resolutions,  
42 more stable numerical schemes and better parameterizations reduce the need for  
43 calibration and the effort required to optimize the numerical parameters. As a  
44 result, the skills required from modelers decrease and forecasts become more  
45 robust. Second, the growing availability of online near-real time data (e.g.,  
46 GEMCO, EMODNET), atmospheric forecasts (e.g., GFS, WRF, ARPEGE) and  
47 large-scale ocean models (e.g., FES2014, CMEMS, HYCOM) provide free  
48  
49  
50  
51  
52  
53  
54  
55  
56  
57  
58  
59  
60  
61  
62  
63  
64  
65

1 access to the information required to force local forecasts worldwide. Third,  
2 large computational infrastructures, both public and commercial, can now  
3 provide the computational power to perform demanding simulations without the  
4 need to acquire and operate these infrastructures. The European Open Science  
5 Cloud (EOSC) and the Partnership for Advanced Computing in Europe  
6 (PRACE) are examples of such public infrastructures.  
7

8  
9 A fourth evolution that can drastically reduce the cost of generating and  
10 operating coastal forecast systems is automation. The recent development of  
11 Web-based platforms that can simultaneously generate and operate coastal  
12 modeling systems with minimal human intervention will reduce the cost of  
13 forecast systems, thereby fostering their dissemination. Examples of these tools  
14 remain scarce in the coastal and ocean communities. WebMARVL (the Virtual  
15 Marine Laboratory, Oke et al., 2016), for setting up ocean circulation and wave  
16 models, Delft-FEWS, dedicated to hydrological and coastal flood forecasting  
17 (Werner et al., 2013), and OPENCoastS, to generate coastal forecast systems for  
18 any location in a few minutes (Oliveira et al. 2020) are the most comprehensive  
19 platforms available. OPENCoastS is a user-friendly platform supported by  
20 EOSC computational services and resources. It is freely available to all users  
21 whereas, for instance, WebMARVL is dedicated to the Australian communities.  
22 The original version of the platform described in Oliveira et al. (2020) was  
23 however limited to simple physics (i.e., 2D depth-averaged shallow water  
24 flows). Now it has matured and addresses more complex flows, including wave  
25 and currents interactions and 3D baroclinic flows. The only inputs requested to  
26 the users to set up a new deployment are the horizontal grid file and, for the 3D  
27 runs, also the vertical grid. The platform is maintained in operation through the  
28 use of European Open Science cloud (EOSC) resources and forecasts still take  
29 only a few minutes to generate.  
30

31 This paper aims at demonstrating how forecast systems built using the  
32 OPENCoastS service can provide accurate prediction of complex flows in  
33 estuarine and coastal environments. “Complex flows” refer here to flows  
34 associated with extreme atmospheric events, breaking waves, and strong density  
35 gradients, and at scales ranging from tens of meters to thousands of kilometers.  
36 Four demonstration examples are presented herein that cover various spatial  
37 scales (from basin-wide to estuarine scales), different forcing agents (tides,  
38 waves, river flow, wind and atmospheric pressure), applied in distinct  
39 geographies (European and Asian coasts). These examples address different  
40 scientific questions (e.g., coastal inundation, salinity dynamics in estuaries) and  
41  
42  
43  
44  
45  
46  
47  
48  
49  
50  
51  
52  
53  
54  
55  
56  
57  
58  
59  
60  
61  
62  
63  
64  
65

the forcing agents include tides, waves, river flow, wind and atmospheric pressure. The criteria behind the selection of the applications are summarized in Table 1. The evolution of the platform, from its original version to its present capabilities, is also detailed to promote the usage of the service software by other teams. It is now freely available under licence Apache License Version 2.0 at <https://gitlab.com/opencoasts/eosc-hub/webportal>.

The paper is organized as follows. First, the OPENCoastS platform is briefly described, with an emphasis on the most recent features. Then, the capabilities of the platform to support operational management in coastal systems are demonstrated through four examples of application. In section 3, these examples are used to illustrate and discuss the lessons learned from the first three years of development of OPENCoastS. Finally, the potential and the present limitations of OPENCoastS are discussed and its evolution is anticipated.

Table 1 - Characterization of the demonstration cases

	<b>Coast of Taiwan</b>	<b>Bay of Biscay</b>	<b>Figueira da Foz Harbor</b>	<b>Tagus Estuary</b>
<b>basin scale</b>	<b>X</b>	<b>X</b>		
<b>coastal/estuarine scale</b>			<b>X</b>	<b>X</b>
<b>2D barotropic</b>	<b>X</b>	<b>X</b>	<b>X</b>	
<b>3D baroclinic</b>				<b>X</b>
<b>waves</b>		<b>X</b>	<b>X</b>	
<b>no waves</b>	<b>X</b>			<b>X</b>

## 2. OPENCoastS service version 2: general description

## 2.1 Overview of the OPENCoastS service

The OPENCoastS service provides accurate circulation forecasts in any coastal system of choice (Oliveira et al., 2020). This is achieved through the use of the process-comprehensive suite of numerical models provided by SCHISM (Zhang et al., 2016), and of a complex computational web platform. SCHISM was chosen because it encompasses all relevant processes, and the web platform was built to run it seamlessly and automates the whole prediction workflow. This combination provides the users the capacity to efficiently build, manage and visualize forecasts. Initially developed as a simple 2D forecast engine (Oliveira et al., 2020), OPENCoastS is now a full-fledged service that simulates all types of estuarine and coastal circulation options: 2D barotropic, 2D waves and currents interaction and 3D baroclinic circulation. Herein, we start by summarizing the architecture and main characteristics of the service and its implementation in the EOSC infrastructure. The implementation of the new circulation functionalities and their dependencies for input file building is detailed afterwards, along with the new options for both ocean forcings and data comparison.

The OPENCoastS service aims at addressing the following properties: Broad availability, Simplicity and user-friendliness, Comprehensiveness, Accuracy and reliability, Flexibility and Modularity (Oliveira et al., 2020). These properties are achieved in the current full circulation service, to guarantee the quality of the final forecasts. Moreover, the architecture to address the properties of modularity and flexibility is paramount to continue to accommodate any new functionalities in the future while maintaining a coherent, simple and user-friendly platform. The service is available at <https://opencoasts.ncg.ingrid.pt> and is organized along the “Configuration assistant”, which guides the assemblage of the site-specific forecast systems; the “Forecast systems manager”, through which users monitor and act upon their forecasts; and the “Outputs viewer” where users visualize and download model’s input and output files (Figure 1). The complete workflow of the Configuration assistant in the OPENCoastS web app is summarized in Figure 2, highlighting the detailed approach to account for the several circulation options requirements.

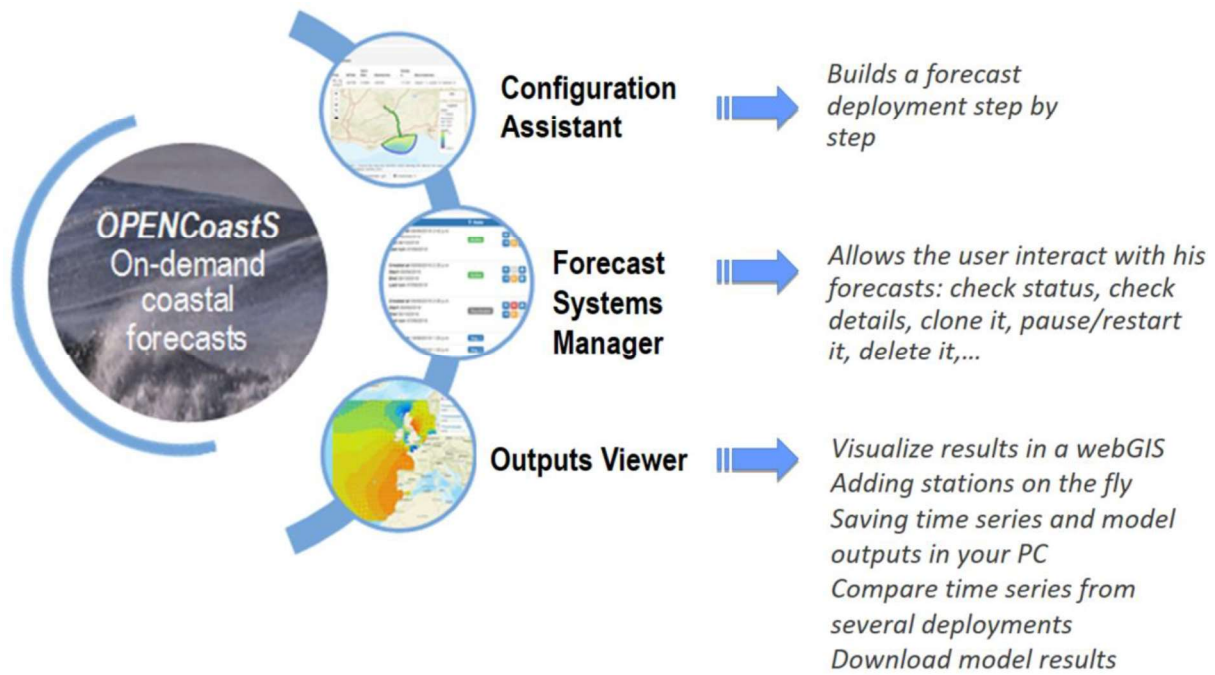


Figure 1: OPENCoastS frontend components

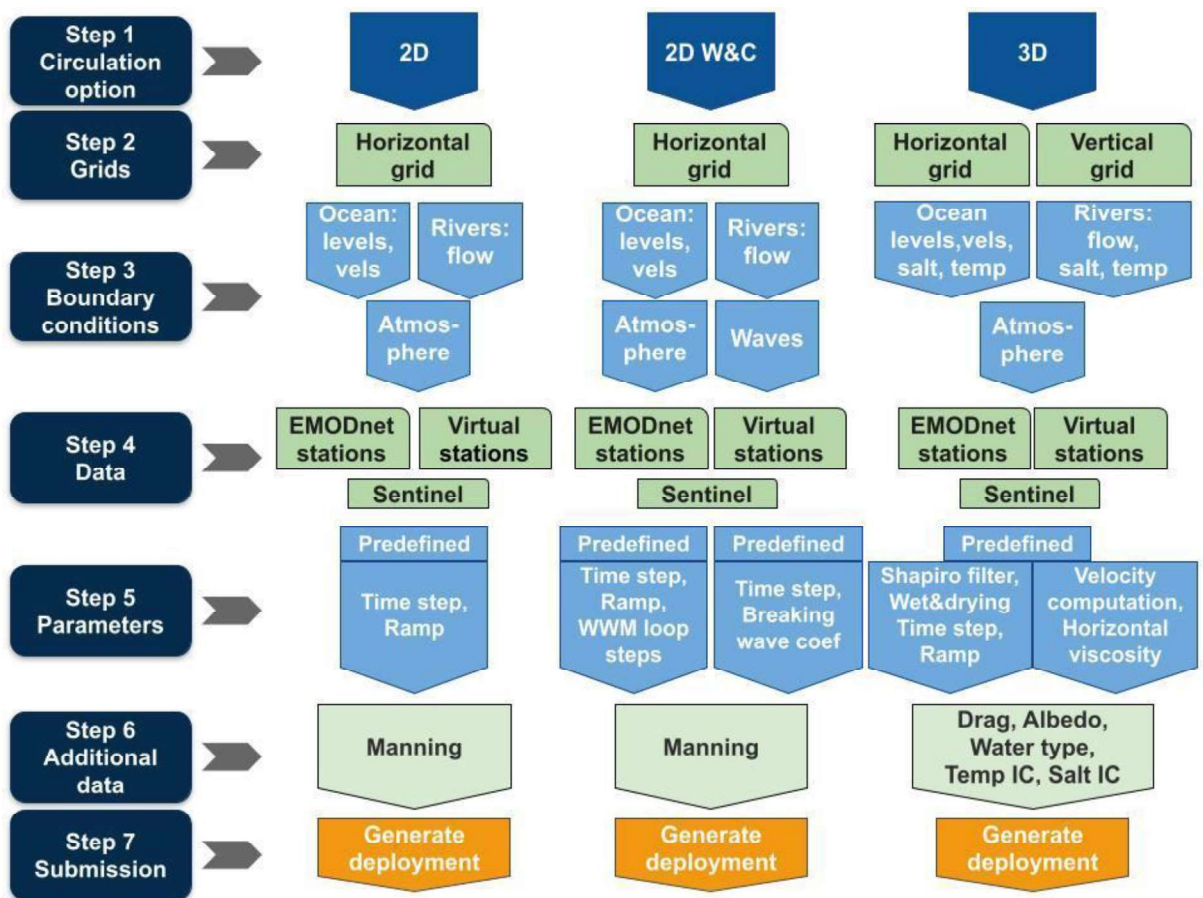


Figure 2. Workflow of the Configuration assistant for the several circulation options.



## 2.2 Current application of SCHISM modeling suite in OPENCoastS

The OPENCoastS evolution to complete coastal physics was made possible by the comprehensive representation of physical processes available in the SCHISM modeling suite (Zhang et al., 2016; <http://ccrm.vims.edu/schismweb>), the open-source modeling engine behind OPENCoastS. SCHISM is an open-source community-supported modeling system designed for a seamless cross-scale simulation from creek to ocean and is used here in version v5.4.1. The model is fully parallelized, to optimize the computing times in forecast applications.

SCHISM has been extensively tested against ocean/coastal benchmarks (Chen et al., 2013; Lynett et al., 2017) and applied to several regional seas, embayments and estuaries worldwide in the fields of general circulation, tsunami, storm-surge and compound inundation, wave-current interaction, water quality, coastal ecology, and morphodynamics (e.g., Guérin et al., 2016; Rodrigues and Fortunato, 2017; Fortunato et al., 2017b; Allen et al., 2018; Li et al., 2018; Du et al., 2020; Wang et al., 2020; Lavaud et al., 2020; Huang et al., 2021). SCHISM is also the hydrodynamic engine of several forecast systems besides OPENCoastS (Stanev et al., 2016; Fortunato et al., 2017a; Chiu et al., 2018; Fernandez-Montblanc et al., 2019).

SCHISM solves the three-dimensional shallow water equations and computes the free-surface elevation and the 3D water velocity, salinity and temperature fields using finite-element and finite-volume schemes. The simultaneous solution of continuity and momentum equations, and a highly efficient semi-implicit finite-element Eulerian-Lagrangian algorithm bypass the most severe stability restrictions (e.g. associated with the Courant number). Mass conservation can be enforced by upwind or finite-volume transport algorithm (TVD2) methods. The natural incorporation of wetting and drying makes the model suitable for inundation studies. In OPENCoastS, the wave model WWM (Roland et al., 2012) is fully coupled in 2DH with SCHISM, and the two models share the same computational grid and domain decomposition. When this option is activated, WWM provides the circulation model with wave forces computed according to the radiation stress formalism of Longuet-Higgins and Stewart (1964) and the circulation model provides WWM with fields of water levels and depth-averaged velocities. SCHISM discretizes the domain using unstructured grids in the horizontal, which allows a greater flexibility in

1 representing the bathymetry, and hybrid SZ coordinates or LSC<sup>2</sup> (Zhang et al.,  
2 2015) along the vertical.

3 In OPENCoastS, only horizontal grids with triangular elements and vertical  
4 grids based on hybrid SZ coordinates can be used, in spite of other  
5 discretization options available in SCHISM. Forcing conditions at the ocean  
6 boundaries in OPENCoastS include both elevation and velocities if FES2014 is  
7 used, providing more accurate results, or just elevations, for the other forcing  
8 options. For 3D simulations, forcing conditions at the oceanic boundaries also  
9 include space and time varying salinity and temperature. At the river  
10 boundaries, forcing conditions can be set up as constant or as time varying.  
11 Those include river flows for 2D simulations and river flows, salinity and  
12 temperature for 3D simulations. OPENCoastS is organized along three  
13 circulation options, depending on the relevant physics. A summary of the inputs  
14 and outputs is presented below along with the new features.  
15  
16  
17  
18  
19  
20  
21  
22

### 23 1) 2D barotropic simulations

24 These simulations output water levels and depth-averaged velocities. The  
25 circulation is forced by tides, wind, atmospheric pressure and river flow. This  
26 option corresponds to the first version of OPENCoastS, with a minor  
27 improvement of forcing both elevation and velocities at the ocean boundaries.  
28 The reader is referred to Oliveira et al. (2020) for further details.  
29  
30  
31  
32  
33  
34

### 35 2) 2D barotropic simulations with wave-current interaction (2D W&C)

36 In addition to Option 1, these simulations also provide wave parameters. All  
37 wave-current interactions are simulated, including the effect of water levels and  
38 depth-averaged currents on wave propagation and the wave forces on the mean  
39 flow through the wave radiation stress gradients. Inside the domain, WWM is  
40 forced by the same surface winds as the circulation model. WWM is also forced  
41 along its open boundaries by time series of directional spectra computed from  
42 an application of the WaveWatch III model (WW3, version 5.16) (The  
43 WAVEWATCH III R Development Group, 2016) to the North Atlantic (grid is  
44 shown in Supplementary material #1). As spectra for larger domains are not  
45 freely available online, this option can only be used for domains forced by  
46 North Atlantic waves. Each deployment has its own WW3 runs, to generate the  
47 necessary boundary conditions. A master WW3 is also maintained to provide  
48 hot-start conditions for each new deployment's forcing WW3 run (Figure 3),  
49 avoiding cold-start conditions or the need to start the forecast deployment  
50  
51  
52  
53  
54  
55  
56  
57  
58  
59  
60  
61  
62  
63  
64  
65

several days in the past. The wave and current backend workflow is highlighted in Figure 3.

current backend workflow is

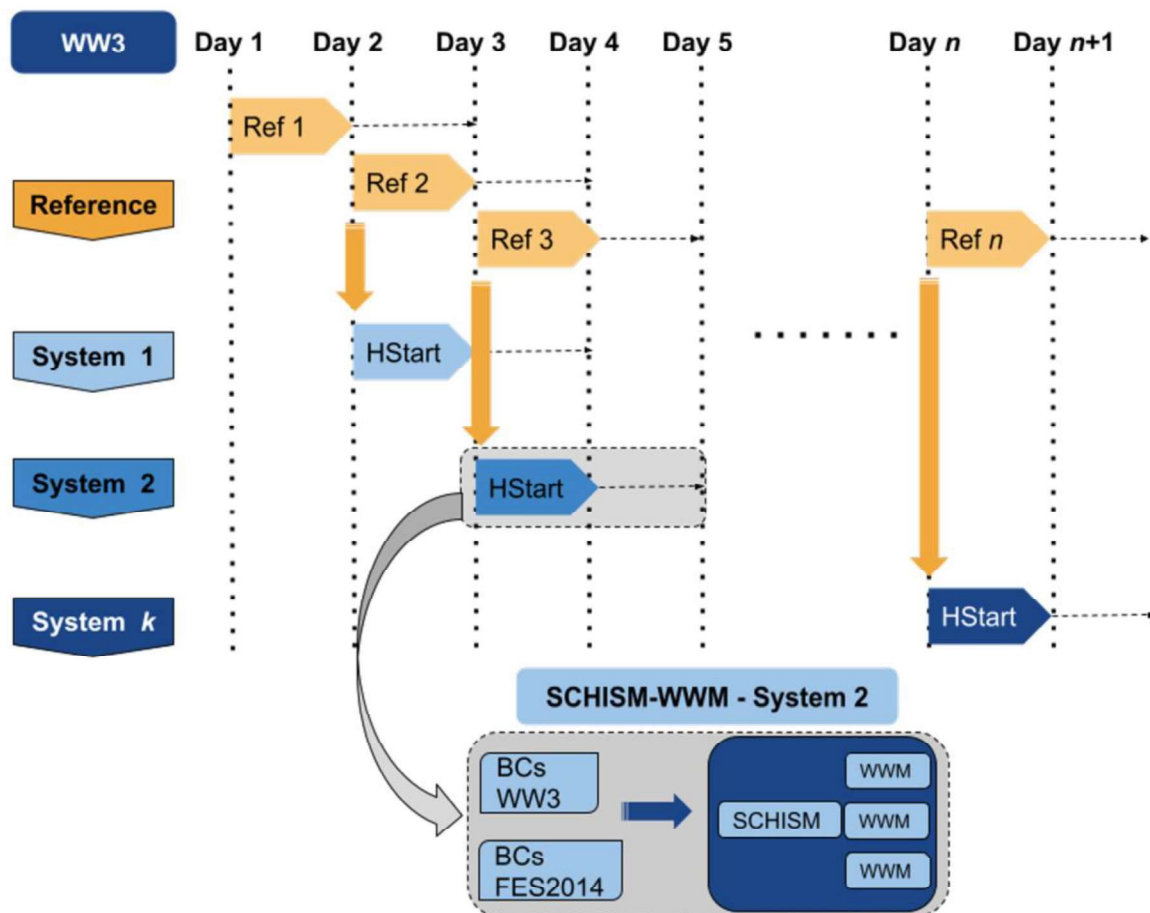


Figure 3: Backend workflow for waves & currents option: procedure for hot starting the waves' simulation. The inset illustrates the procedure for each simulation, with the possibility of having multiple WWM runs for one time step of SCHISM or the opposite situation.

3) 3D baroclinic simulations - these simulations provide 3D fields of velocity, salinity and water temperature, besides water levels. They can be forced by tides, river flow, temperature and salinity at all the boundaries, and also by the atmospheric surface forcing (wind, air temperature, pressure, humidity, solar radiation and downwelling longwave radiation).

Boundary conditions for 3D velocities, salinity and temperature at the ocean boundaries are provided by CMEMS (<https://marine.copernicus.eu/>), with two sources available: CMEMS Global and Iberian-Biscay-Ireland (IBI) regional seas. These sources can also be used to force water elevations in other

1 circulation options as part of the ocean boundary conditions portfolio.  
2 Atmospheric inputs for these runs can be obtained with GFS or WRF, both  
3 provided by NOAA. At the rivers' boundaries, besides annual and monthly  
4 values, a web provider for time series can also be used to provide flow forecasts  
5 every day. Finally, one river flow can also be specified as a percentage of  
6 another one, either defined as monthly or annual values or through an external  
7 river forecast provider.  
8  
9

10  
11  
12 Unlike the wave and current interaction option, 3D baroclinic forecasts can  
13 be generated anywhere in the world. The forcing of the salinity and temperature  
14 ocean boundaries can only be done with one of the two CMEMS options:  
15 Global or IBI.  
16  
17  
18

19  
20 The Forecast systems manager provides multiple actions on forecasts 1)  
21 conclude deployment; 2) pause and cancel a deployment and 3) cloning a  
22 deployment, besides monitoring the status of the runs and providing alerts for  
23 the near conclusion of the operating period. The cloning facility is used  
24 frequently as it provides a very efficient way to perform sensitivity analyses on  
25 parameters and forcings for a specific site.  
26  
27  
28  
29

30  
31 The Outputs viewer presents results from all circulation options. Besides the  
32 inclusion of the new variables depending on the type of deployment selected,  
33 the capacity to see 3D results along the vertical (and to compare different levels)  
34 was also added. Downloading facilities were extended for the new files  
35 generated in the additional options.  
36  
37  
38  
39

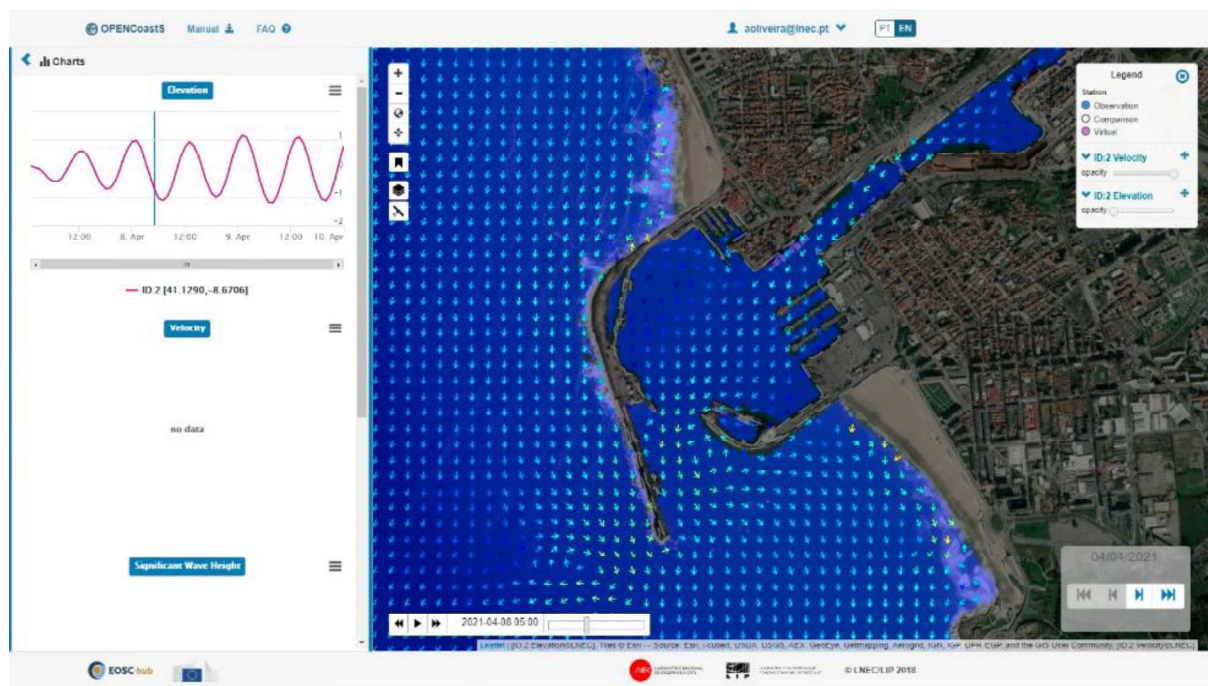
## 40 41 2.3 Data comparison options in OPENCoastS 42

43 Automatic comparison with field data validates the quality of the predictions  
44 and supports the usefulness of the tool and the users' confidence in its results.  
45 OPENCoastS is linked to the EMODNET Physics elevation data hub  
46 (<https://portal.emodnet-physics.eu/>). The user selects the stations for the  
47 model/data comparison for each deployment in the Configuration assistant and  
48 then visualizes the data against the results in the viewer.  
49  
50  
51  
52

53  
54 Comparison with remote sensing data is also available, to determine the  
55 interface between land and water (extent of inundation), based on images from  
56 the Sentinel satellites. The possibility of comparing model results with a  
57 processed Sentinel image is integrated in the Configuration assistant. If the user  
58  
59  
60  
61  
62  
63  
64  
65

1 selects the comparison with remote sensing option, the OPENCoastS workflow  
2 starts a regular procedure to download images from the ESA Copernicus  
3 OpenHub, crops them to the limits of the deployment horizontal grid, binarizes  
4 it to determine the land-water interface and converts it to a raster. The rasters  
5 are stored in a database and are connected to the respective deployment ID.  
6 Upon entering the viewer page, the OPENCoastS interface builds a JSON file  
7 with the latest rasters.  
8  
9

10  
11  
12 In the viewer, the users can select the visualization of the Sentinel-based layers  
13 against the model results. As Sentinel images have a specific time stamp, we  
14 provide the capacity to overlap each simulation with the nearest processed  
15 image. This visual comparison is available for the whole simulation, regardless  
16 of the specific time step that would be closest to the Sentinel time stamp. The  
17 rasters are loaded into the map with an opacity applied to them to facilitate the  
18 comparison with the model forecasts (Figure 4).  
19  
20  
21  
22  
23  
24



25  
26  
27  
28  
29  
30  
31  
32  
33  
34  
35  
36  
37  
38  
39  
40  
41  
42  
43  
44  
45  
46  
47  
48  
49 Figure 4 - Comparison between the water limit extracted from Sentinel 2 images  
50 (in blue) and the OPENCoastS prediction (velocity field). The brown dashed  
51 line marks the limit of the grid, which represents the Leixões harbor and  
52 Matosinhos Beach in Northern Portugal.  
53  
54

55  
56  
57 New satellite images are downloaded and added to the system at the beginning  
58 of each day. Upon selecting the option to download the images, as there will not  
59  
60  
61  
62  
63  
64  
65

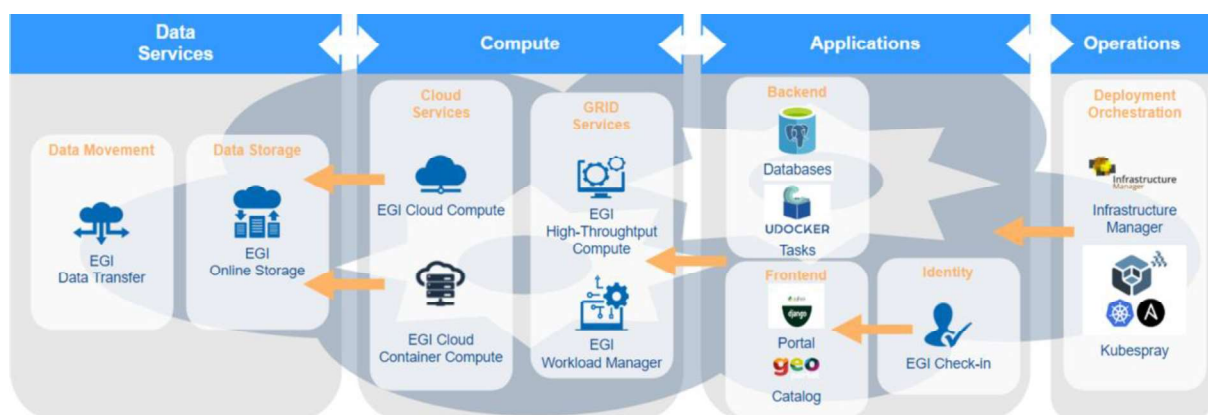
1 be any images available on the database, OPENCoastS checks back in time to  
2 retrieve the images available from the last five days.  
3  
4

## 5 2.4 Brief description of the implementation of OPENCoastS in the 6 EOSC infrastructure 7

8  
9 During the last decade, Global Open Science emerged as a trusted digital  
10 platform to support the scientific community. The European project EOSC-hub  
11 aimed to foster the best practices for data and services management, simplifying  
12 the researchers' access to available infrastructure sites. OPENCoastS is one of  
13 the seven thematic services integrated in the EOSC infrastructure in the scope of  
14 this project (<https://marketplace.eosc-portal.eu/services/opencoasts-portal>).  
15  
16

17 The OPENCoastS service requires high availability of computational resources  
18 to guarantee the delivery of forecast outputs in due time. Portugal's National  
19 Distributed Computing Infrastructure (INCD) and Cantabria Physics Institution  
20 (IFCA) offer the required facilities for OPENCoastS simulations, providing the  
21 integration with the core EOSC-hub services for authentication, accounting,  
22 computation and data preservation.  
23  
24

25 OPENCoastS comprehends several components, such as catalogs of model  
26 data/results and their metadata, SCHISM processing scripts, a web  
27 Configuration assistant, a web portal for managing the user accounts and  
28 applications, and a web map visualization tool. These components were  
29 integrated with the EOSC core services summarized in Figure 5. Available core  
30 services were promoted within EOSC-hub to support OPENCoastS and other  
31 thematic services ([https://marketplace.eosc-portal.eu/services/c/access-physical-  
32 infrastructures](https://marketplace.eosc-portal.eu/services/c/access-physical-infrastructures)).  
33  
34  
35  
36  
37  
38  
39  
40  
41  
42



57 Figure 5. OPENCoastS integration with EOSC services  
58  
59  
60  
61  
62  
63  
64  
65

1 The main supporters of those core services are the European Grid Initiative  
2 (EGI), for cloud and grid services, and EUDAT for storage. Authentication  
3 Authorization and Identity (AAI) is available in both EUDAT and EGI  
4 portfolios, which implement the AARC Blueprint Architecture ([https://aarc-  
5 project.eu/architecture/](https://aarc-project.eu/architecture/)), supporting communities users' with subordinate end  
6 services.  
7

8  
9 The current implementation of OPENCoastS in the INCD infrastructure uses the  
10 following core services: EGI Cloud Compute, EGI Online Storage and EGI  
11 Check-in for AAI. These EOSC core services enable the deployment of the  
12 OPENCoastS applications and provide the endpoint for the portal. Additionally,  
13 SCHISM's processing work and all related tasks are submitted to EGI  
14 Workload Manager. This manager distributes the computational demand by all  
15 available resource sites using EGI High-Throughput Compute. The software  
16 requirements and dependencies are encapsulated in a docker image that is  
17 loaded in the computing nodes with the udocker tool (Gomes et al., 2018).  
18 Udocker allows pulling and executing docker containers in Linux batch systems  
19 and interactive clusters in user space without requiring root privileges. A bundle  
20 that encapsulates the whole OPENCoastS service and its installation at a user-  
21 defined infrastructure is freely distributed at the GitLab repository in  
22 <https://gitlab.com/opencoasts/eosc-hub/webportal>.  
23  
24  
25  
26  
27  
28  
29  
30  
31  
32  
33

### 3. OPENCoastS applications

#### 3.1. Extreme water levels in the coast of Taiwan

34  
35  
36  
37  
38  
39  
40 The northwestern Pacific Ocean is the most active tropical cyclone basin on  
41 Earth (Elsner and Liu, 2003). The most severe of these cyclones, locally known  
42 as typhoons, can generate extreme storm surges that can have devastating  
43 effects on the shores of the Philippines, China, Taiwan and Japan. Here, we  
44 illustrate the generation of a forecast system for the coast of Taiwan with  
45 OPENCoastS and its validation using only publicly available data.  
46  
47

48 Typhoon tracks can be divided into three groups (Elsner and Liu, 2003). Taiwan  
49 is affected by typhoons following two of these groups: the straight track, a  
50 general westward path, and the parabolic recurving track, which follows to the  
51 North-west and then turns north. The model domain (Figure 6) was thus defined  
52 such that it contains these typhoon tracks. The coastal boundary was defined  
53 using the Global Self-consistent, Hierarchical, High-resolution Shoreline  
54 database ([https://gnome.orr.noaa.gov/goods/tools/GSHHS/coast\\_subset](https://gnome.orr.noaa.gov/goods/tools/GSHHS/coast_subset)), and  
55  
56  
57  
58  
59  
60  
61  
62  
63  
64  
65

1 the bathymetry was extracted from the General Bathymetric Chart of the Oceans  
 2 (<https://download.gebco.net>). A grid with 93,000 nodes was generated by  
 3 automatically placing the nodes with a specified spatially-varying resolution  
 4 using the program xmgredit (Turner and Baptista, 1993). This resolution varies  
 5 between 1-2 km around Taiwan and 10-16 km in the deep ocean. Then, this  
 6 preliminary grid was automatically improved using the program nicegrid  
 7 (Fortunato et al., 2011). The resulting number of elements linked to each node  
 8 varies between 5 and 7 to ensure a smooth transition between element sizes.  
 9 Because the domain is very deep, friction is expected to be negligible. The  
 10 Manning coefficient was set to  $0.022 \text{ m}^{1/3}/\text{s}$  throughout the domain, and the  
 11 model was not calibrated. The time step was specified as 240 s, as proposed by  
 12 OPENCoastS.

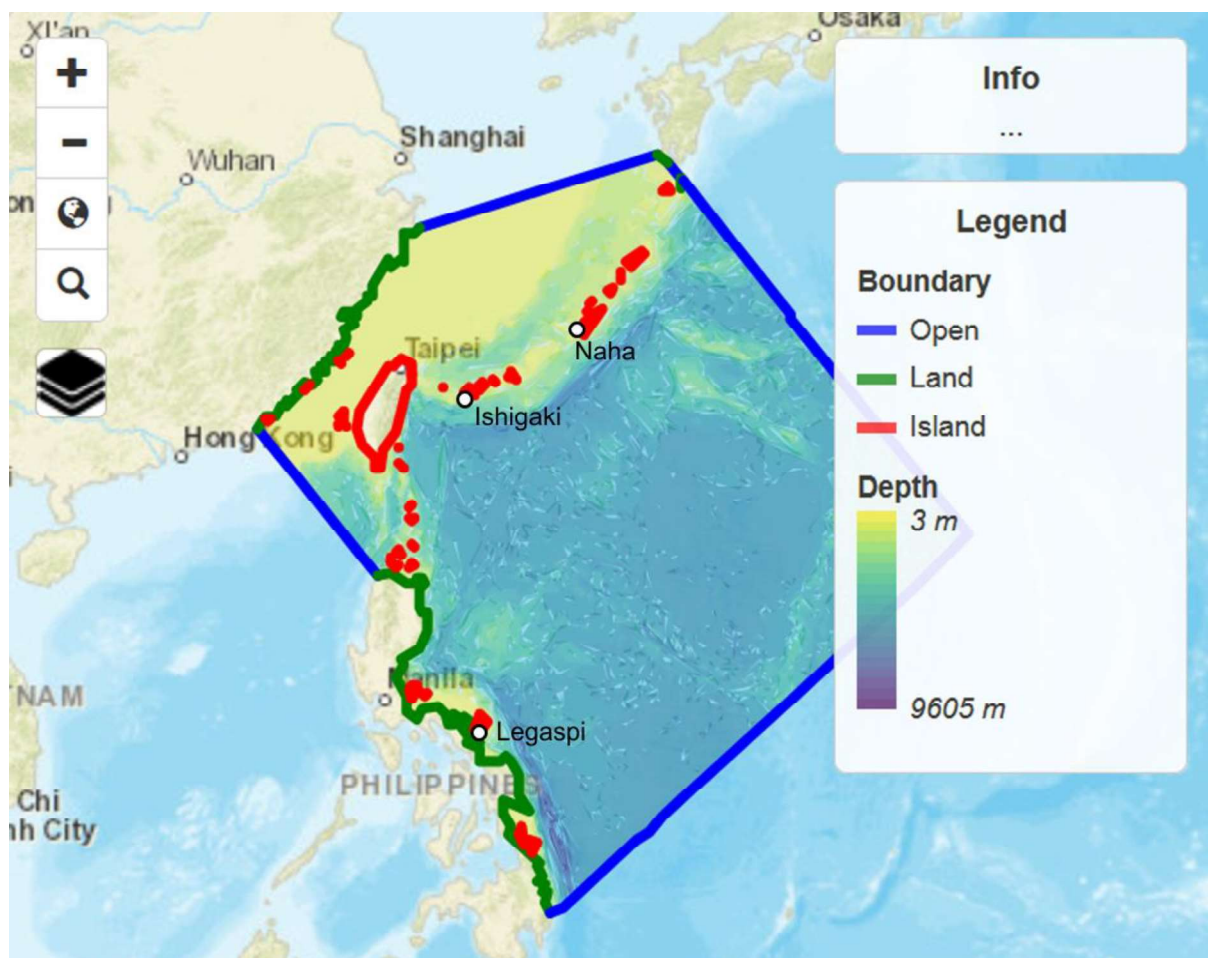


Figure 6. Taiwan typhoon model domain, bathymetry and tide gauges (circles)



SCHISM was forced at the sea surface by winds and atmospheric pressure from GFS, and at the open boundaries by tides from FES2014 (Lyard et al., 2020) and the inverse barometer effect.

Forecasts were produced in OPENCoastS for the 2020 typhoon season (July to September). During this period, 14 tropical storms occurred in the Pacific, including typhoons Hagupit (July 31 – August 5), Bavi (August 21 – August 27), Maysak (August 27 – September 3) and Haishen (August 31 – September 9). Haisen, in particular, peaked as a Category 4 typhoon. The model was validated using sea surface height data from the three stations located within the domain (Figure 6) and available at the EMODnet platform. The data time series include numerous gaps.

Table 2. Validation of the Taiwan forecasts: unbiased root mean square errors (URMSE) and normalized unbiased root mean square errors (NURMSE). NURMSE are normalized by the standard deviation of the data.

Station	Ishigaka	Legaspi	Naha
URMS (m)	0.10	0.05	0.07
NURMS (%)	25	12	14

Comparison with field data shows that the model reproduces sea surface heights with unbiased root mean square errors between 5 and 10 cm (Table 2). These errors correspond to 12 to 25% of the standard deviation of the measured sea surface height. The RMSE obtained with OPENCoastS compare favorably with a recent application to the same area (Liu and Huang, 2020).

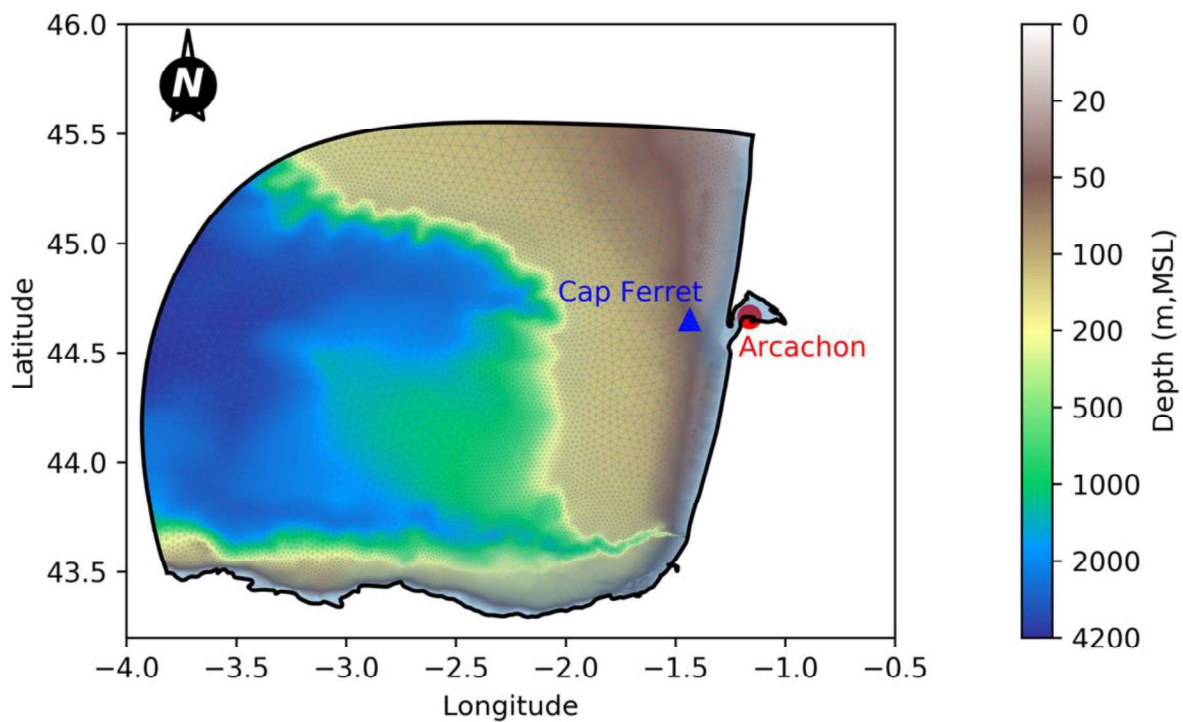
The model accuracy could certainly be improved. A comparison between the shoreline database and satellite images shows that the data are coarse and outdated in some areas. Calibration of the friction coefficient in the continental shelf between Taiwan and China, which would require tide gauge data in that area, would probably improve the water levels prediction locally. More importantly, including waves would increase the storm surge. The importance of waves on storm surges was shown by Chen et al. (2017) for this particular region, and is also shown in the next section for the Bay of Biscay.

In spite of these limitations, this application shows that adequate forecasts can be quickly obtained with OPENCoastS without any a priori knowledge of the

1 study region and using only open data and model results for the model setup and  
2 validation.  
3  
4

### 5 3.2. Storm waves and surge in the Bay of Biscay 6

7 The Bay of Biscay is exposed to severe winter storms, which can drive waves of  
8 significant height (hereafter  $H_s$ ) over 10 m, storm surges over 1.5 m (Bertin et  
9 al., 2015; Lavaud et al., 2020) and catastrophic marine flooding (Bertin et al.,  
10 2014). The storm Justine hit the central part of the Bay of Biscay on 31st of  
11 January 2021 and drove waves of  $H_s$  reaching 10 m in the deep ocean and over  
12 8 m at the nearshore buoy Cap Ferret (Figure 7). Inside the Arcachon Lagoon  
13 (Figure 8), water level measurements suggest that a storm surge of about 1.0 m  
14 developed. In this section, we present a fully-coupled 2DH high resolution  
15 forecast of the sea state and water levels associated with this storm to  
16 demonstrate the relevance of short waves in OPENCoastS.  
17  
18  
19  
20  
21  
22  
23  
24



49 Figure 7. Bathymetric map and extension of the computational domain  
50 with location of the Arcachon tide gauge (red circle) and the Cap Ferret buoy  
51 (blue triangle).  
52

53 The unstructured grid used to perform the forecast covers the southern part of  
54 the Bay of Biscay (Figure 7) and comprises 60060 nodes and 117303 triangular  
55 elements, with a spatial resolution ranging from 5500 m along the open  
56 boundary to 80 m at the entrance of the Arcachon Lagoon. Along the open  
57  
58  
59  
60  
61  
62  
63  
64  
65

boundary, the circulation model was forced by amplitudes and phases of the 34 main tidal constituents from FES2014 (Lyard et al., 2020). Over the whole domain, the circulation model was forced by 10 m wind speed and sea-level pressure issued from ARPEGE atmospheric forecasts and an inverse barometer condition was applied along the open boundary. ARPEGE wind fields were also used to force the wave model WWM. Along the open boundary, WWM was forced by time-series of directional wave spectra, which were computed from WW3 forced with wind fields from the GFS atmospheric model. The time steps were set to 30 s and 300 s in the hydrodynamic and wave model, respectively.

The model predictions were first compared against observed significant wave height ( $H_s$ ), mean absolute wave period ( $T_{m02}$ ) and mean wave direction ( $Mwd$ ) available at the Cap Ferret Buoy, located 14 km from the coast by a mean water depth of 50 m. This comparison reveals that  $H_s$  and  $T_{m02}$  are very well reproduced, with normalized root mean square errors (NRMSE) of 12 and 8 %, respectively.  $Mwd$  is also well reproduced, with a root mean square error (RMSE) lower than  $5^\circ$  (Figure 8).

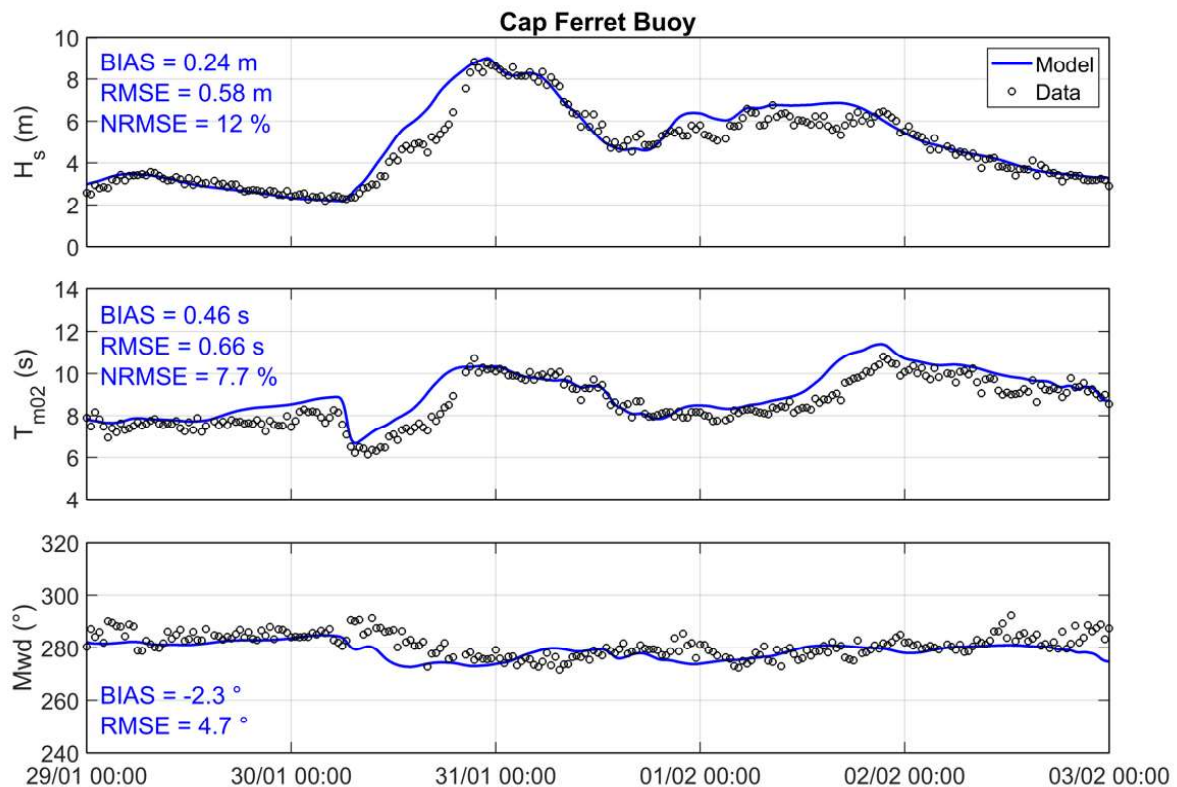


Figure 8. Modeled (blue) against observed (black circles) significant wave height ( $H_s$ ), mean absolute wave period ( $T_{m02}$ ) and mean wave direction ( $Mwd$ ) at Cap Ferret Buoy during storm Justine. Normalized root mean square errors (NRMSE) are normalized by the mean of the data.

Water levels were measured inside the Arcachon Lagoon (Figure 9) and the storm surge was computed as the difference between the observations and a tidal prediction based on a harmonic analysis performed over a 5-year time series using U-Tide (Codiga, 2011). For the model, the storm surge was computed as the difference between simulations including tides and surge and a simulation that is forced only by tides. The comparison between observed and modeled storm surges reveals firstly that without wave forces, the model underestimates the surge peak by a factor of 3. When short waves are included in the simulation, this strong negative bias is cancelled out and the RMSE is reduced by a factor of 3 (Figure 9). For the total water level, including short waves also removes a 0.27 m negative bias and reduces the RMSE by a factor of 3. This behavior was already observed by Lavaud et al. (2020), for the storm Klaus (2009), and explained by the dissipation of storm waves at the entrance of the Arcachon Lagoon, which drives a large wave setup that extends at the scale of the whole lagoon. This new application demonstrates that the results of Lavaud et al. (2020) were not specific to a particular storm and suggest that short waves should be included in storm surge forecasts when intense wave breaking occurs at the entrance of estuaries and lagoons.

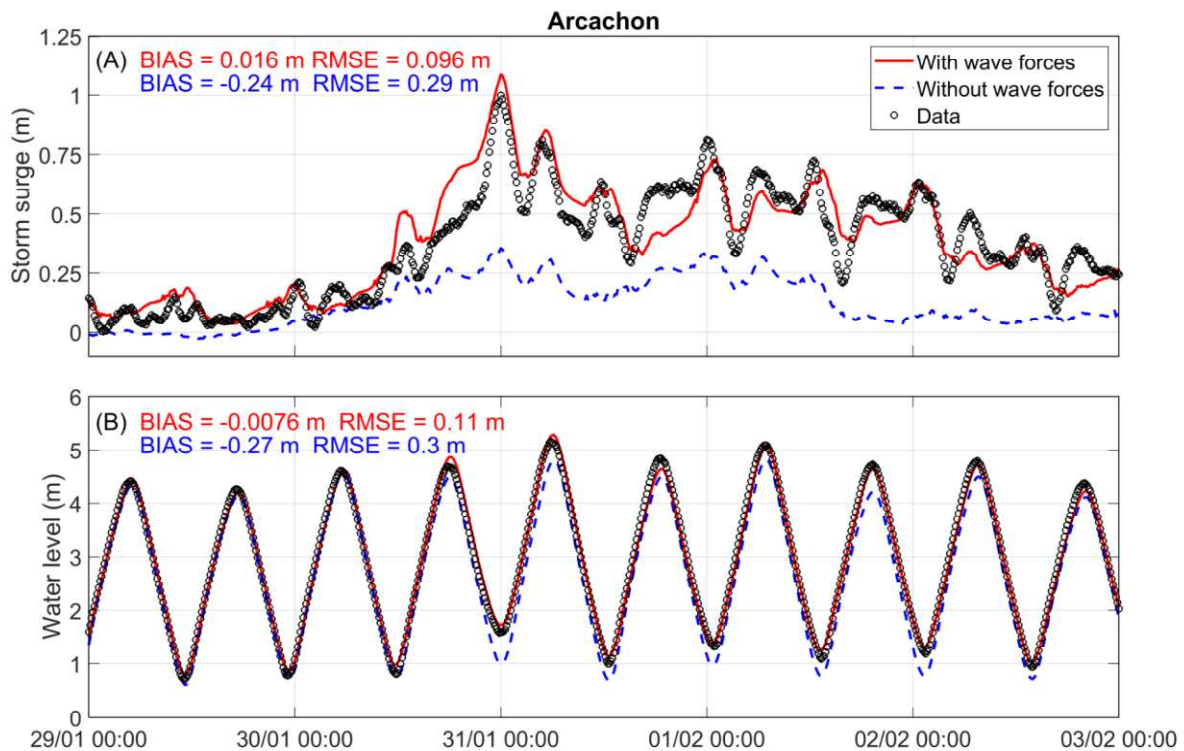


Figure 9. (A) Observed (black circles) against modeled storm surge with (blue) and without (red) short waves and (B) same for total water levels.

### 3.3. Impacts of bathymetric changes on forecasted nearshore circulation at Figueira da Foz

#### 3.3.1. Motivation and goals

In nearshore areas, short-term predictions of coastal hydrodynamics are useful for harbor navigation, bathing safety and civil protection. Because these areas are shallow, the hydrodynamic conditions can be affected by bathymetric changes. These changes can occur rapidly due to both natural and anthropogenic causes, such as storm-driven erosion or dredging and deposition. Thus, the accuracy of model predictions could depend on frequent updates of the bathymetry.

To assess this dependence, sensitivity tests to observed bathymetric evolutions were performed near a jettied tidal inlet on the western coast of Portugal. These tests were made using an OPENCoastS forecast, and illustrate how the platform can be exploited for hindcast runs. Indeed, these hindcast runs were done using the input files created and made available through the forecast runs. The forecast was initially implemented for the nearshore area in the vicinity of the harbor of Figueira da Foz (Figure 10a), following the 2D W&C workflow (Figure 2). The unstructured grid has about 50,000 nodes and extends from 84 m water depth offshore to 14 km upstream the Mondego estuary; the grid spatial resolution ranged from 2.5 km offshore to 20 m in the nearshore area and along stream, and the timestep was set to 30 seconds. The forecast system (Nahon et al., 2020) was implemented in OPENCoastS with a bathymetry surveyed in the summer 2019 (ebb-tidal delta and subtidal sandbars) and March 2020 (intertidal beach). The model skill is evaluated for offshore and nearshore significant wave height, and nearshore, harbor and river water level elevation and is summarized in Table 3.

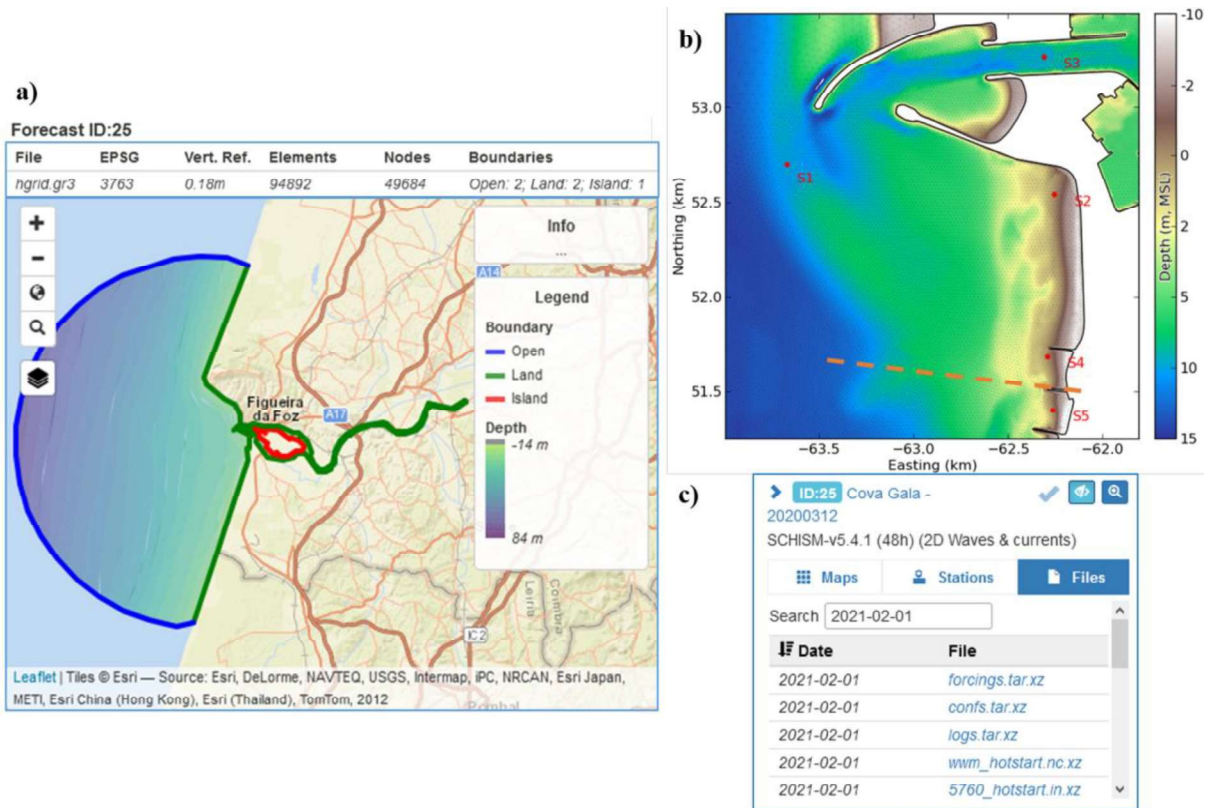


Figure 10. Figueira da Foz Forecast system: a) computational domain as seen in OPENCoastS; b) Cova Gala Beach, south of the harbor entrance, with the location of the output stations (S1-S5) and of the bathymetric profile shown in Figure 11a (dashed orange line); c) OPENCoastS tool to download daily files containing forcings, hotstarts and model results.

Table 3. Bias and root mean square errors (RMSE) between modeled and observed significant wave height ( $H_s$ ) and water level elevation across the computational domain (after Nahon et al., 2020)

	$H_s$		Elevation	
	Bias (% of mean)	RMSE (% of mean)	Bias (m)	RMSE (m)
Offshore: Wave buoy	-13.4	20.4	-	-
Nearshore: Pressure transducers	-17.3 < . < 12.4	13.9 < . < 20.0	0.13 < . < 0.26	0.14 < . < 0.26
Harbor: Tidal gauge	-	-	-0.01	0.04
Upstream: Tidal gauge	-	-	-0.07	0.12

### 3.3.2. Measured bathymetric changes

The sensitivity of the model results to the bathymetry was assessed considering two bathymetries in addition to the one from 2019/20 used in the forecast system. The first bathymetry was used to investigate the consequence of the inflow of sediments from the beach and sandbars to the north of the inlet's northern jetty. During storms, this inflow of sediments can rapidly accrete the access channel (S1 location, Figure 10b), as, for example, during the storm Epsilon in October 2020 (Figure 11b). A post-Epsilon survey, made on 6 November 2020, was then used to modify the reference bathymetry and assess the impacts on waves and current predictions.

In recent years, the sand brought in by (storm) waves is dredged and deposited in front of Cova Gala Beach, to the south of the inlet's southern jetty. In 2018, these deposits created a protuberance of the ebb-tidal delta. Initially within 6 m to 10 m depth (chart datum), the deposit subsequently spread and evolved into large nearshore sandbars visible in the 2019 bathymetry (Figure 11a). In the second bathymetry, the nearshore area was changed to a state representative of summer 2018.

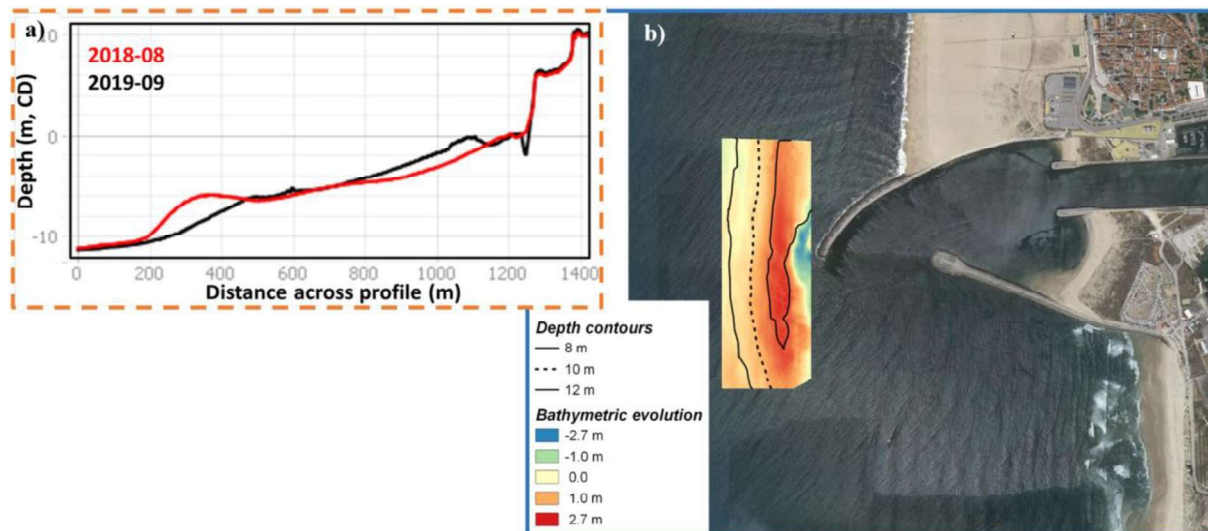


Figure 11. Bathymetric evolution near Figueira da Foz harbor: a) bathymetric evolution of the 2018 dredging disposal (red) through to 2019 (black), along the profile plotted on Figure 10b (dashed orange line); b) bathymetric evolution of the harbor entrance channel during storm Epsilon (October, 2020) along with post-storm depth contours (positive is accretion).

### 3.3.3. Duplicated forecasts and hydrodynamic results

All input files and forcings were downloaded from the OPENCoastS service web app using the Files download tool accessible within the Outputs viewer (Figure 10c): input files from 1 February 2021 were used with circulation initial conditions created on 31 January 2021. The model was then run offline for the three bathymetric configurations.

Simulations were analyzed at five virtual output stations (Figure 10b), although here results were outputted every 10 min compared to 1 hour outputs within OPENCoastS. Stations S1-S3 were placed to evaluate the sensitivity of the harbor hydrodynamics to bathymetric changes induced by storm Epsilon. Stations S4-S5 were placed shoreward of the 2018 sediment disposal location to analyze the impact of the dredging spoils on the beach hydrodynamics.

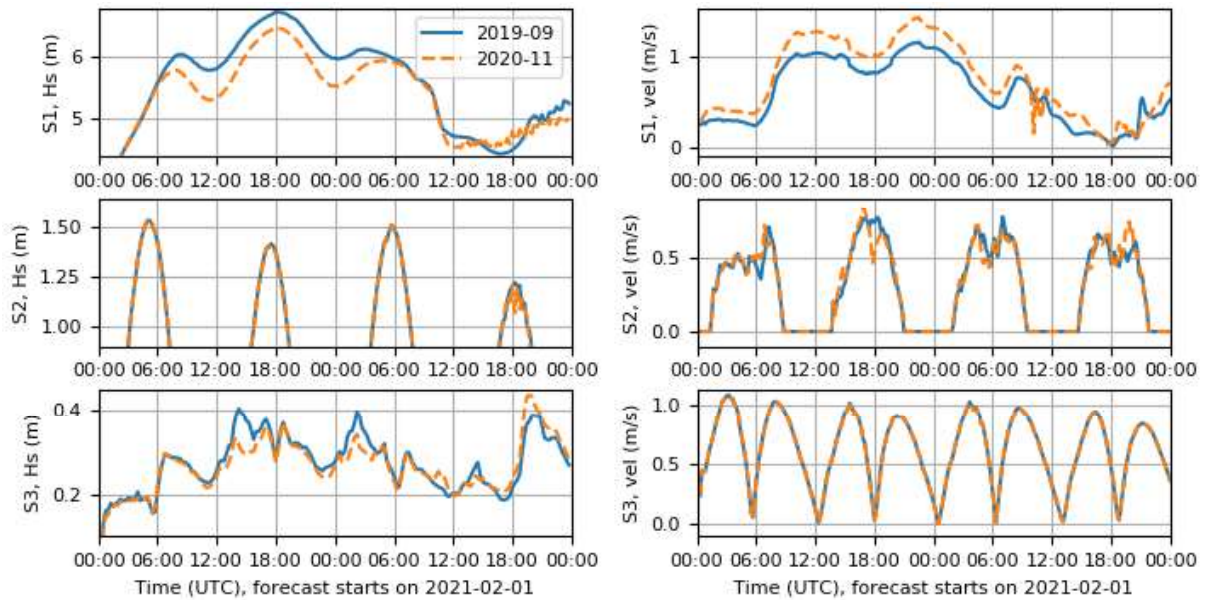
The simulated period covered the 2nd storm modeled in the previous case study in the Bay of Biscay. Here, the offshore significant wave height peaked at 6.9 m at 15:00 on 1 February, before the high tide of a moderate 2.5 m tidal cycle. At stations S1-S3, the main differences concerned the significant wave height and the current velocities, and were largest within the access channel (S1, Figure 12). At S1, compared to the configuration with a well-defined channel, the post-storm configuration showed a modest decrease of 5% of the significant wave height at the peak of the storm and a stronger increase of the current velocities, on the order of 20%. Differences at the beach (S2, 0 m depth MSL) are less pronounced, likely because the surfzone was saturated and the wave height was controlled by the depth-induced breaking. In the 9-m deep main harbor channel (S3), differences in velocities were negligible. In contrast, the wave height was affected by up to 25% although this concerned waves with a modest size. However, phase-averaged models such as WWM only provide an approximate representation of wave diffraction which may limit the accuracy of the wave predictions between the jetties. Also, WWM does not reproduce the wave reflection at the jetties.

Stations S4-S5 were placed along the 0 m depth contour, southward of the tidal inlet. Similarly to S2, differences in significant wave height were negligible. Differences in total water level reached 5 cm (Figure 13). The main differences at those beach cells were observed in the intensity of the modeled current, with overall stronger currents, after the deposited sediment migrates shoreward (2019-09 configuration).

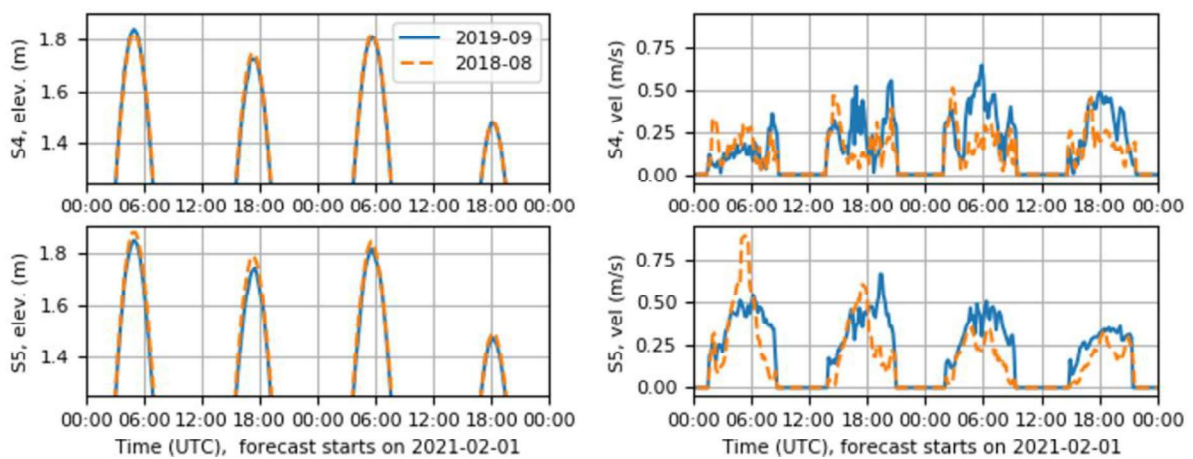
Overall, these results show that, although the bathymetric changes were significant, differences were modest in terms of modeled significant wave



1 height and total water levels. The main differences occurred for the predicted  
 2 current velocities in the access channel (S1) and over the intertidal beach in the  
 3 shadow of the dredging spoils (S4 and S5). However, these results cannot be  
 4 generalized since this analysis was made under specific wave and tidal  
 5 conditions.  
 6  
 7



8  
 9  
 10  
 11  
 12  
 13  
 14  
 15  
 16  
 17  
 18  
 19  
 20  
 21  
 22  
 23  
 24  
 25  
 26  
 27  
 28 Figure 12. Sensitivity of the significant wave height (Hs, left) and current  
 29 velocities (right) to storm-driven bathymetric evolutions in late October 2020.  
 30  
 31  
 32

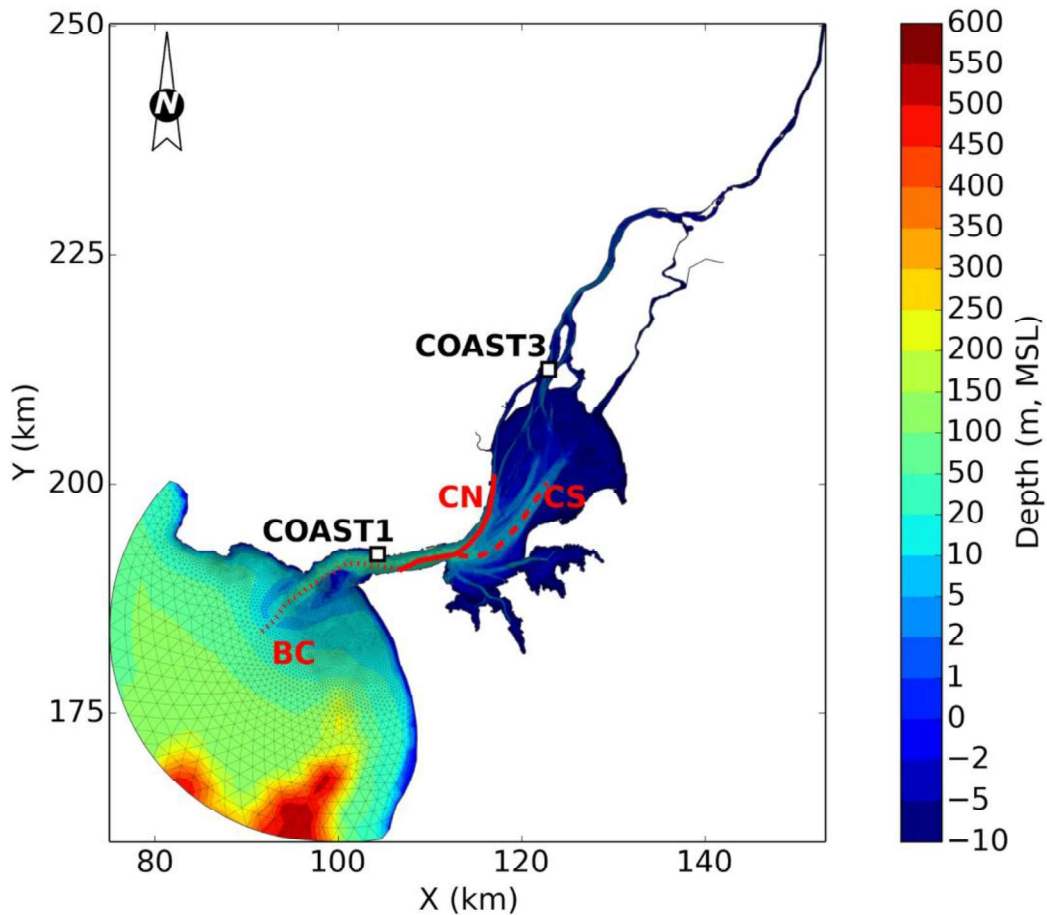


33  
 34  
 35  
 36  
 37  
 38  
 39  
 40  
 41  
 42  
 43  
 44  
 45  
 46  
 47  
 48  
 49  
 50  
 51  
 52  
 53  
 54  
 55  
 56  
 57  
 58  
 59  
 60  
 61  
 62  
 63  
 64  
 65  
 66  
 67  
 68  
 69  
 70  
 71  
 72  
 73  
 74  
 75  
 76  
 77  
 78  
 79  
 80  
 81  
 82  
 83  
 84  
 85  
 86  
 87  
 88  
 89  
 90  
 91  
 92  
 93  
 94  
 95  
 96  
 97  
 98  
 99  
 100  
 101  
 102  
 103  
 104  
 105  
 106  
 107  
 108  
 109  
 110  
 111  
 112  
 113  
 114  
 115  
 116  
 117  
 118  
 119  
 120  
 121  
 122  
 123  
 124  
 125  
 126  
 127  
 128  
 129  
 130  
 131  
 132  
 133  
 134  
 135  
 136  
 137  
 138  
 139  
 140  
 141  
 142  
 143  
 144  
 145  
 146  
 147  
 148  
 149  
 150  
 151  
 152  
 153  
 154  
 155  
 156  
 157  
 158  
 159  
 160  
 161  
 162  
 163  
 164  
 165  
 166  
 167  
 168  
 169  
 170  
 171  
 172  
 173  
 174  
 175  
 176  
 177  
 178  
 179  
 180  
 181  
 182  
 183  
 184  
 185  
 186  
 187  
 188  
 189  
 190  
 191  
 192  
 193  
 194  
 195  
 196  
 197  
 198  
 199  
 200  
 201  
 202  
 203  
 204  
 205  
 206  
 207  
 208  
 209  
 210  
 211  
 212  
 213  
 214  
 215  
 216  
 217  
 218  
 219  
 220  
 221  
 222  
 223  
 224  
 225  
 226  
 227  
 228  
 229  
 230  
 231  
 232  
 233  
 234  
 235  
 236  
 237  
 238  
 239  
 240  
 241  
 242  
 243  
 244  
 245  
 246  
 247  
 248  
 249  
 250  
 251  
 252  
 253  
 254  
 255  
 256  
 257  
 258  
 259  
 260  
 261  
 262  
 263  
 264  
 265  
 266  
 267  
 268  
 269  
 270  
 271  
 272  
 273  
 274  
 275  
 276  
 277  
 278  
 279  
 280  
 281  
 282  
 283  
 284  
 285  
 286  
 287  
 288  
 289  
 290  
 291  
 292  
 293  
 294  
 295  
 296  
 297  
 298  
 299  
 300  
 301  
 302  
 303  
 304  
 305  
 306  
 307  
 308  
 309  
 310  
 311  
 312  
 313  
 314  
 315  
 316  
 317  
 318  
 319  
 320  
 321  
 322  
 323  
 324  
 325  
 326  
 327  
 328  
 329  
 330  
 331  
 332  
 333  
 334  
 335  
 336  
 337  
 338  
 339  
 340  
 341  
 342  
 343  
 344  
 345  
 346  
 347  
 348  
 349  
 350  
 351  
 352  
 353  
 354  
 355  
 356  
 357  
 358  
 359  
 360  
 361  
 362  
 363  
 364  
 365  
 366  
 367  
 368  
 369  
 370  
 371  
 372  
 373  
 374  
 375  
 376  
 377  
 378  
 379  
 380  
 381  
 382  
 383  
 384  
 385  
 386  
 387  
 388  
 389  
 390  
 391  
 392  
 393  
 394  
 395  
 396  
 397  
 398  
 399  
 400  
 401  
 402  
 403  
 404  
 405  
 406  
 407  
 408  
 409  
 410  
 411  
 412  
 413  
 414  
 415  
 416  
 417  
 418  
 419  
 420  
 421  
 422  
 423  
 424  
 425  
 426  
 427  
 428  
 429  
 430  
 431  
 432  
 433  
 434  
 435  
 436  
 437  
 438  
 439  
 440  
 441  
 442  
 443  
 444  
 445  
 446  
 447  
 448  
 449  
 450  
 451  
 452  
 453  
 454  
 455  
 456  
 457  
 458  
 459  
 460  
 461  
 462  
 463  
 464  
 465  
 466  
 467  
 468  
 469  
 470  
 471  
 472  
 473  
 474  
 475  
 476  
 477  
 478  
 479  
 480  
 481  
 482  
 483  
 484  
 485  
 486  
 487  
 488  
 489  
 490  
 491  
 492  
 493  
 494  
 495  
 496  
 497  
 498  
 499  
 500  
 501  
 502  
 503  
 504  
 505  
 506  
 507  
 508  
 509  
 510  
 511  
 512  
 513  
 514  
 515  
 516  
 517  
 518  
 519  
 520  
 521  
 522  
 523  
 524  
 525  
 526  
 527  
 528  
 529  
 530  
 531  
 532  
 533  
 534  
 535  
 536  
 537  
 538  
 539  
 540  
 541  
 542  
 543  
 544  
 545  
 546  
 547  
 548  
 549  
 550  
 551  
 552  
 553  
 554  
 555  
 556  
 557  
 558  
 559  
 560  
 561  
 562  
 563  
 564  
 565  
 566  
 567  
 568  
 569  
 570  
 571  
 572  
 573  
 574  
 575  
 576  
 577  
 578  
 579  
 580  
 581  
 582  
 583  
 584  
 585  
 586  
 587  
 588  
 589  
 590  
 591  
 592  
 593  
 594  
 595  
 596  
 597  
 598  
 599  
 600  
 601  
 602  
 603  
 604  
 605  
 606  
 607  
 608  
 609  
 610  
 611  
 612  
 613  
 614  
 615  
 616  
 617  
 618  
 619  
 620  
 621  
 622  
 623  
 624  
 625  
 626  
 627  
 628  
 629  
 630  
 631  
 632  
 633  
 634  
 635  
 636  
 637  
 638  
 639  
 640  
 641  
 642  
 643  
 644  
 645  
 646  
 647  
 648  
 649  
 650  
 651  
 652  
 653  
 654  
 655  
 656  
 657  
 658  
 659  
 660  
 661  
 662  
 663  
 664  
 665  
 666  
 667  
 668  
 669  
 670  
 671  
 672  
 673  
 674  
 675  
 676  
 677  
 678  
 679  
 680  
 681  
 682  
 683  
 684  
 685  
 686  
 687  
 688  
 689  
 690  
 691  
 692  
 693  
 694  
 695  
 696  
 697  
 698  
 699  
 700  
 701  
 702  
 703  
 704  
 705  
 706  
 707  
 708  
 709  
 710  
 711  
 712  
 713  
 714  
 715  
 716  
 717  
 718  
 719  
 720  
 721  
 722  
 723  
 724  
 725  
 726  
 727  
 728  
 729  
 730  
 731  
 732  
 733  
 734  
 735  
 736  
 737  
 738  
 739  
 740  
 741  
 742  
 743  
 744  
 745  
 746  
 747  
 748  
 749  
 750  
 751  
 752  
 753  
 754  
 755  
 756  
 757  
 758  
 759  
 760  
 761  
 762  
 763  
 764  
 765  
 766  
 767  
 768  
 769  
 770  
 771  
 772  
 773  
 774  
 775  
 776  
 777  
 778  
 779  
 780  
 781  
 782  
 783  
 784  
 785  
 786  
 787  
 788  
 789  
 790  
 791  
 792  
 793  
 794  
 795  
 796  
 797  
 798  
 799  
 800  
 801  
 802  
 803  
 804  
 805  
 806  
 807  
 808  
 809  
 810  
 811  
 812  
 813  
 814  
 815  
 816  
 817  
 818  
 819  
 820  
 821  
 822  
 823  
 824  
 825  
 826  
 827  
 828  
 829  
 830  
 831  
 832  
 833  
 834  
 835  
 836  
 837  
 838  
 839  
 840  
 841  
 842  
 843  
 844  
 845  
 846  
 847  
 848  
 849  
 850  
 851  
 852  
 853  
 854  
 855  
 856  
 857  
 858  
 859  
 860  
 861  
 862  
 863  
 864  
 865  
 866  
 867  
 868  
 869  
 870  
 871  
 872  
 873  
 874  
 875  
 876  
 877  
 878  
 879  
 880  
 881  
 882  
 883  
 884  
 885  
 886  
 887  
 888  
 889  
 890  
 891  
 892  
 893  
 894  
 895  
 896  
 897  
 898  
 899  
 900  
 901  
 902  
 903  
 904  
 905  
 906  
 907  
 908  
 909  
 910  
 911  
 912  
 913  
 914  
 915  
 916  
 917  
 918  
 919  
 920  
 921  
 922  
 923  
 924  
 925  
 926  
 927  
 928  
 929  
 930  
 931  
 932  
 933  
 934  
 935  
 936  
 937  
 938  
 939  
 940  
 941  
 942  
 943  
 944  
 945  
 946  
 947  
 948  
 949  
 950  
 951  
 952  
 953  
 954  
 955  
 956  
 957  
 958  
 959  
 960  
 961  
 962  
 963  
 964  
 965  
 966  
 967  
 968  
 969  
 970  
 971  
 972  
 973  
 974  
 975  
 976  
 977  
 978  
 979  
 980  
 981  
 982  
 983  
 984  
 985  
 986  
 987  
 988  
 989  
 990  
 991  
 992  
 993  
 994  
 995  
 996  
 997  
 998  
 999  
 1000

### 3.4. Tagus estuary 3D baroclinic case study

1 The Tagus estuary (Portugal) is one of the largest estuaries in Europe and holds  
2 a major natural reserve, which is one of the most important sanctuaries for  
3 wintering or staging birds. The estuarine margins are intensively occupied, with  
4 a population of about one million inhabitants, and support diverse uses and  
5 activities (urban, industrial/harbors, agriculture, shellfish harvesting). The  
6 estuary has a deep and narrow inlet channel and a broad and shallow inner  
7 basin. The intertidal area constitutes about 40% of the total estuarine surface  
8 (Castanheiro, 1986). Tides are the main driver of the circulation in the Tagus  
9 estuary (Fortunato et al., 2017b). Tides are semi-diurnal and range from 0.55 m  
10 to 3.86 m at the coast (Guerreiro et al., 2015). The tidal propagation within the  
11 estuary is complex and tidal amplitudes are amplified by resonance (Fortunato  
12 et al., 1997, 1999). Other drivers, such as the river flow, wind, atmospheric  
13 pressure and surface waves, also influence the circulation within the estuary.  
14 The Tagus River, with an average flow of 370 m<sup>3</sup>/s (APA, 2012), is the main  
15 source of freshwater into the estuary. Other tributaries (the Sorraia and the  
16 Trancão rivers) also contribute to the freshwater inflow into the estuary. The  
17 estuary is usually well-mixed, but stratification can occur at high flow rates and  
18 low tidal ranges (Neves, 2010; Rodrigues and Fortunato, 2017). Residence  
19 times in the estuary result from the interaction between different factors, such as  
20 tide, river flow and wind (e.g., Oliveira and Baptista, 1997; Vaz and Dias,  
21 2014). Several studies showed the interaction between the Tagus and the  
22 adjacent coastal area and the sediments, nutrients, plankton and fisheries  
23 dynamics in the estuary (e.g., Gameiro and Brotas, 2010; Valente and Silva,  
24 2009). The physical drivers play an important role in these dynamics. In the  
25 Tagus estuary, residence time is the main factor influencing phytoplankton  
26 annual variability (Brotas and Gameiro, 2009), with lower concentrations  
27 occurring during wet years. Moreover, other physical factors, such as salinity  
28 can influence the biotic distribution within the estuaries (e.g. Wolf et al., 2009).  
29 The operational model of the Tagus estuary was first implemented and validated  
30 in hindcast mode (Rodrigues and Fortunato, 2017). The model extends from the  
31 ocean to the river and the domain is discretized with a horizontal grid of  
32 about 83,000 nodes and 157000 elements, which has a typical resolution of 15-  
33 25 m (Figure 14). The vertical domain is discretized with a hybrid grid with 39  
34 SZ levels (30 S levels in the upper 100 m, and 9 Z levels between 100 m and the  
35 maximum depth). Within OPENCoastS (Figure 15) the model is forced by: i)  
36 sea surface heights, salinity, water temperature from the CMEMS-IBI model at  
37 the oceanic boundary; ii) extrapolation of river flows from the SNIRH Almourol  
38  
39  
40  
41  
42  
43  
44  
45  
46  
47  
48  
49  
50  
51  
52  
53  
54  
55  
56  
57  
58  
59  
60  
61  
62  
63  
64  
65

1 station (<http://snirh.apambiente.pt>), zero salinity and monthly climatological  
2 values of water temperature at the riverine boundaries (Tagus and Sorraia  
3 rivers); and iii) atmospheric data at the surface from the GFS model. The time  
4 step was set to 30s.  
5  
6  
7  
8



41  
42  
43  
44  
45  
46  
47

Figure 14. Horizontal grid and location of the stations. The Almourol station, used to provide river boundary conditions, is located about 37 km upstream of the model domain

48  
49  
50  
51  
52  
53  
54  
55  
56  
57

Data from the COASTNET Portuguese monitoring network (<http://geoportal.coastnet.pt/>) were used to assess the operational model salinity and water temperature. The data-model comparison was performed between November 2019 and February 2020, which includes a period of high river flows susceptible to lead to stratification (Rodrigues and Fortunato, 2017), aiming to assess the operational model response for different forcing conditions.

58  
59  
60  
61  
62  
63  
64  
65

Results show the ability of the model to represent the main variations regarding salinity and water temperature, both upstream and downstream (Figure 16,

1 supplementary material #2). However, the temperature is underestimated  
2 upstream, where a negative bias is observed (Figure 16, supplementary material  
3 #2). RMSE and mean absolute error (MAE) for salinity and water temperature  
4 (Figure 16) are typically of the same order of magnitude of previous hindcast  
5 applications (Rodrigues and Fortunato, 2017; Rodrigues et al., 2019), although  
6 slightly higher upstream. The differences observed between the data and the  
7 model forecasts may be due to the boundary conditions imposed. At the riverine  
8 boundaries, the river flow is extrapolated from the last flow measured, which  
9 may introduce phase errors in the model results (of about 1-2 days) when  
10 significant variations of the flow occur. Also, the water temperature at these  
11 boundaries is based on climatology, which constitutes a major source of  
12 uncertainty and may explain the larger differences observed in the upstream  
13 station. The atmospheric forcing may also influence the salinity and water  
14 temperature dynamics in the Tagus estuary (Rodrigues et al., 2016 and  
15 Rodrigues and Fortunato, 2017) and explain some of the differences observed,  
16 since a global model with a low resolution was used.

17  
18  
19  
20  
21  
22  
23  
24  
25  
26 The 3D model is able to represent the vertical dynamics of salinity and water  
27 temperature in the Tagus estuary, which is expected to become stratified for  
28 river flows higher than 1000 m<sup>3</sup>/s. The operational model represents the  
29 stratified conditions (Figure 17 and Figure 18) that occur during a period where  
30 river flow was about 2000 m<sup>3</sup>/s. Results show that the riverine plume extends  
31 further into the ocean for larger river flows and leads to the stratification of the  
32 water column, with salinities near the inlet of about 20 at the surface and about  
33 32-34 near the bottom at low tide. For a river flow of about 370 m<sup>3</sup>/s (close to  
34 the mean river flow of the Tagus river - 360 m<sup>3</sup>/s) the mixing is stronger; near  
35 the inlet salinity ranges between 30-34 at low tide.

36  
37  
38  
39  
40  
41  
42 Overall the forecasts proved to adequately represent the salinity and water  
43 temperature dynamics in the Tagus estuary and can provide useful information  
44 to support diverse activities in the area.  
45  
46  
47  
48  
49  
50  
51  
52  
53  
54  
55  
56  
57  
58  
59  
60  
61  
62  
63  
64  
65

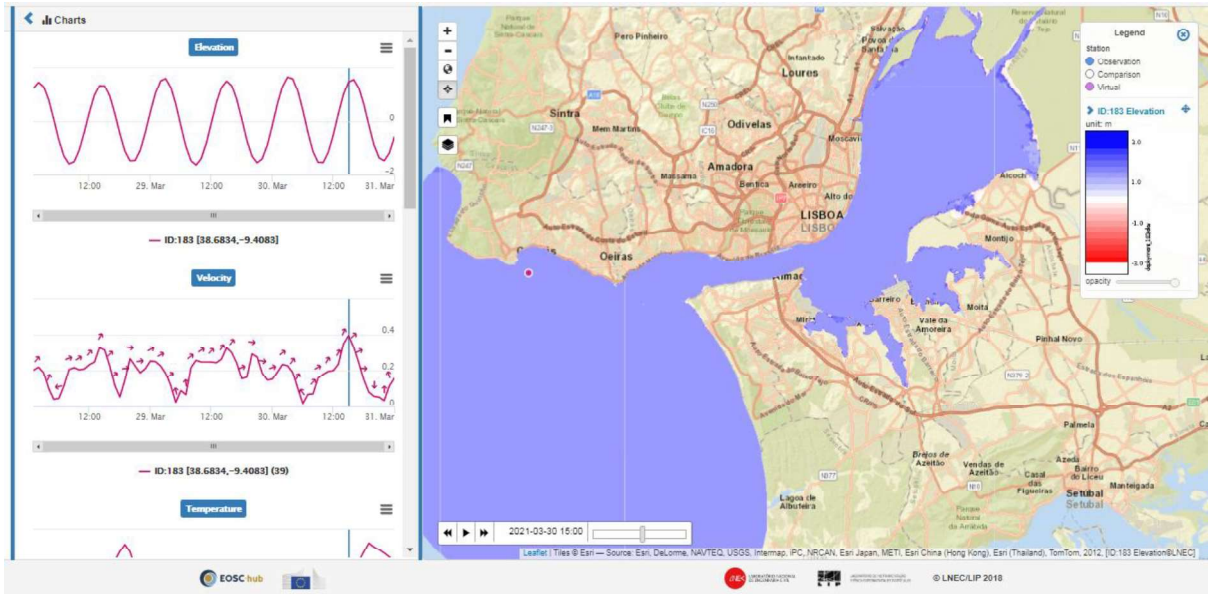


Figure 15. Outputs viewer: Water levels and velocities at Cascais - Tagus estuary. The time series of water levels and velocities on the left were extracted at the red circle outside the mouth.

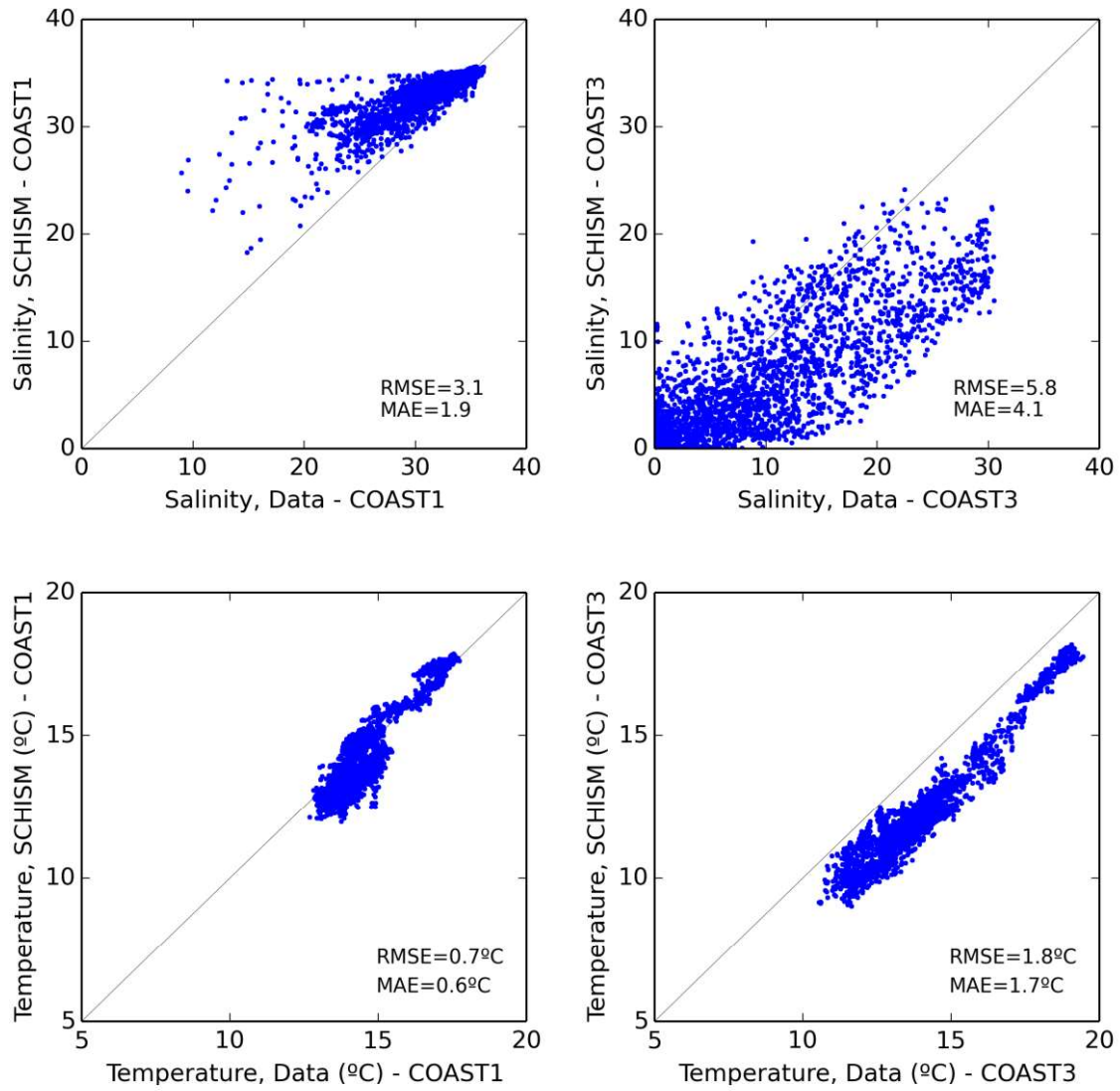
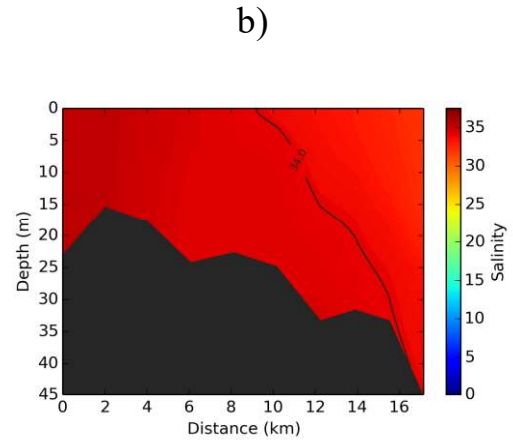
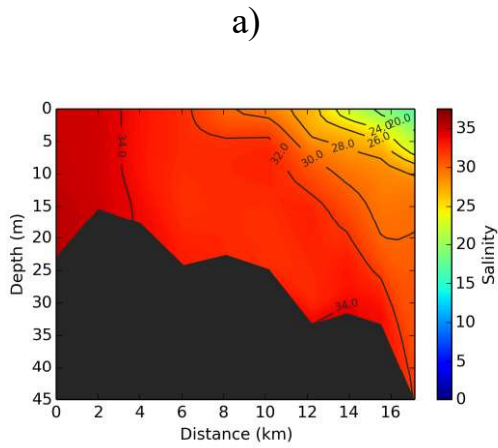
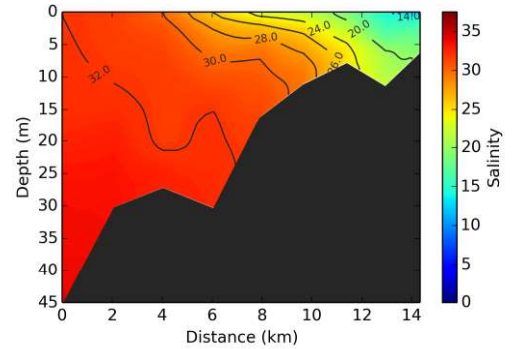
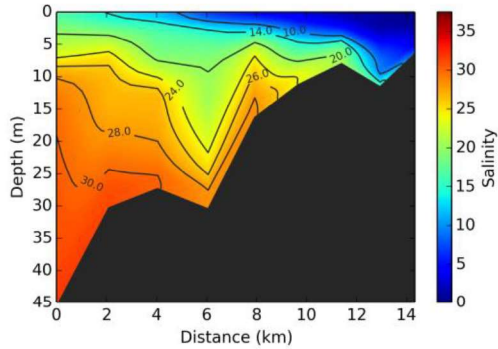


Figure 16. Salinity and water temperature data vs SCHISM Forecasts in the Tagus estuary. Root mean square error (RMSE) and mean absolute error (MAE) for salinity and water temperature are indicated in the figures.

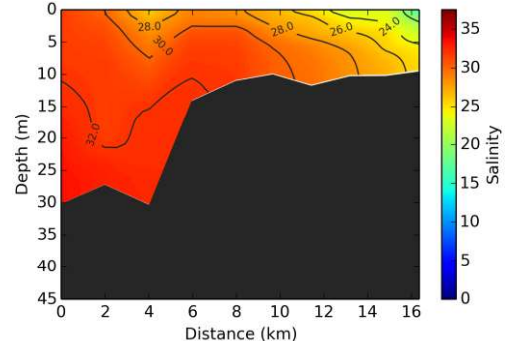
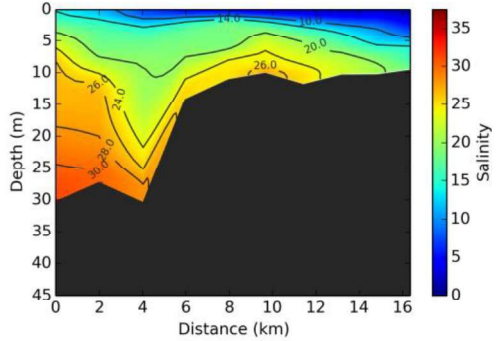
1  
2  
3 Barra-  
4 Corred  
5 or  
6  
7  
8  
9



16  
17 Cala do  
18 Norte  
19  
20  
21  
22  
23  
24  
25  
26  
27

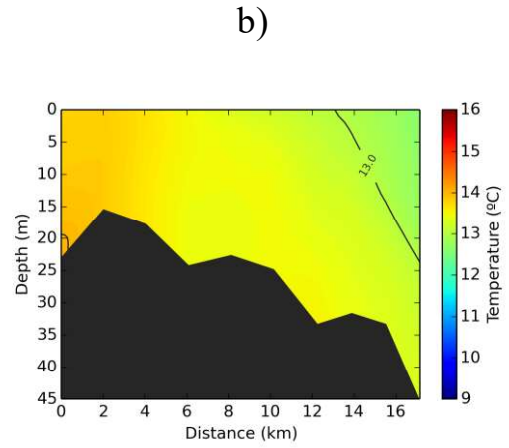
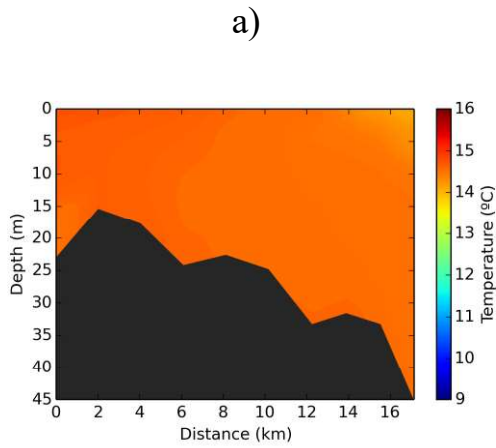


30  
31 Cala de  
32 Samora  
33  
34  
35  
36  
37  
38  
39  
40  
41  
42  
43  
44

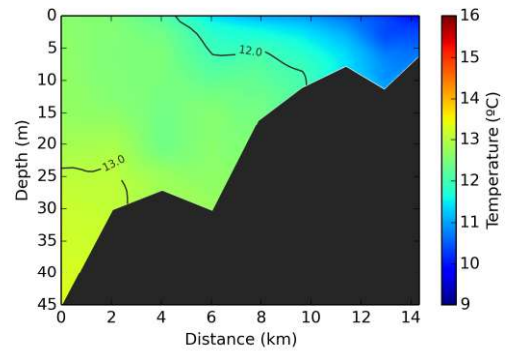
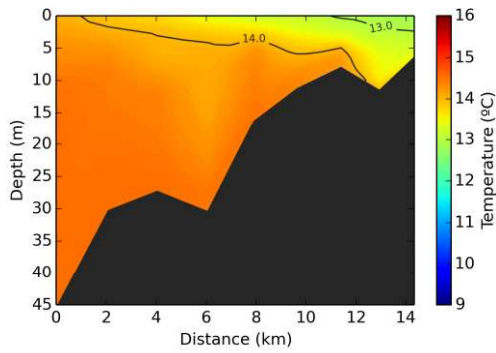


45  
46 Figure 17. Forecasted vertical profiles of salinity at low tide on a) December 23,  
47 2019 - estimated river flow of 2000 m<sup>3</sup>/s and b) January 25, 2020 - estimated  
48 river flow of 370 m<sup>3</sup>/s (see Figure 14 for the location of the longitudinal  
49 profiles).  
50  
51  
52  
53  
54  
55  
56  
57  
58  
59  
60  
61  
62  
63  
64  
65

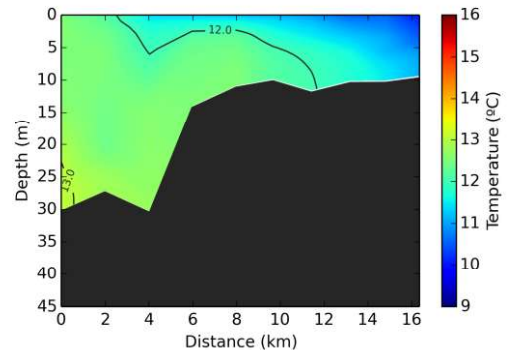
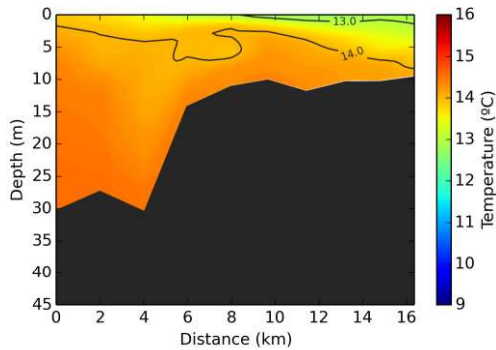
1  
2  
3 Barra-  
4 Corred  
5 or  
6  
7  
8  
9



16  
17 Cala do  
18 Norte  
19  
20  
21  
22  
23  
24  
25  
26  
27



28  
29  
30  
31 Cala de  
32 Samora  
33  
34  
35  
36  
37  
38  
39  
40  
41  
42  
43  
44



45  
46 Figure 18. Forecasted vertical profiles of water temperature on December 23,  
47 2019 and on January 25, 2020, at low tide (see Figure 14 for the location of the  
48 longitudinal profiles).  
49  
50  
51  
52  
53  
54  
55  
56  
57  
58  
59  
60  
61  
62  
63  
64  
65



## 4. Discussion, conclusions and future perspectives

Over the past three years, OPENCoastS has grown from an innovative on-demand platform that addressed simple 2D barotropic forecasts to a powerful tool that solves all circulation options, used by over 400 users and applied on all continents. Most past applications are scientific ones, to understand the importance of processes at a site or to explore the influence of numerical and physical parameters or forcing sources on forecasts, among other goals. Several deployments were also built to predict site circulation, either to support field work preparation or to anticipate hazardous conditions.

The applications presented herein proved the usefulness of OPENCoastS and provided important lessons. The application to the coast of Taiwan showed that useful forecasts can be obtained using only large-scale public data. This success is very important, considering the existence of many data-poor environments worldwide without forecast systems. Also, this forecast was run with simplified physics (i.e., waves were neglected). Although this simplification is still common in forecast systems (Umgiesser et al., in press), waves can play an important role in the storm surge (Lavaud et al., 2020; Liu and Huang, 2020). This role is confirmed in the Bay of Biscay application, where the inclusion of wave forces reduces the error in the storm surge by a factor of 3. To a smaller extent, the accuracy of the forecasts in shallow areas also depends on accurate and updated bathymetries. This dependence is illustrated in the Figueira da Foz harbor example. The limitations imposed by the lack of detailed data is also highlighted in the Tagus Estuary case, which suggests that absence of small-scale atmospheric predictions and river flow forecasts constitute important sources of errors. In summary, while OPENCoastS can provide useful results using only publicly available data and simplified physics, the more demanding users should include high-resolution and updated data, and include all the relevant processes. The possibility to use atmospheric predictions provided by the user is planned for future versions of OPENCoastS, similar to the current capacity to specify a source for river flow predictions.

The applications presented herein also highlight the usefulness of OPENCoastS as a tool to automate many time-consuming tasks in coastal modeling, such as the generation of input files, downloading and processing of atmospheric forecast and post-processing of model results. This automation fosters the use of models for sensitivity analyses, as illustrated by the Bay of Biscay application.

1 Although OPENCoastS was designed to generate forecasts, the Figueira da Foz  
2 harbor application shows how it can be exploited for hindcasts, taking  
3 advantage of the automatic generation of input files.  
4

5  
6 In spite of OPENCoastS only requiring an unstructured computational grid to  
7 set up a new forecast, the availability of such grids remains a limitation for  
8 many users, in particular for those outside the academic fora. Recent  
9 developments in automatic grid generation (e.g., Roberts et al., 2019), along  
10 with the availability of global bathymetry services, have paved the way for an  
11 integration of a grid generator in the configuration assistant of OPENCoastS.  
12 The robustness of the computational engine SCHISM, even for highly skewed  
13 grids and noisy bathymetries, is paramount for the success of this task, bearing  
14 in mind the need to include the necessary grid features for a good simulation,  
15 depending on the simulation type (e.g. good representation of the channel cross-  
16 sections and dikes).  
17  
18  
19  
20  
21  
22  
23  
24

25 While forecasts are often much more difficult to build than simple offline  
26 applications of a specific model, thus justifying the development of  
27 sophisticated on-demand platforms such as OPENCoastS, these two tasks share  
28 a common need in high-resolution runs. These runs can be either for  
29 applications to very large domains (regional or global modeling), spatially very  
30 small events (e.g. discharge of an outfall) or multiple runs (e.g. scenarios  
31 simulation), but they all require very large computational resources. Moreover,  
32 a user-friendly platform may significantly reduce the learning curve on how to  
33 use a new model and to build on-the-fly boundary conditions from several  
34 sources. Therefore, hincast or scenario simulations are now being integrated in  
35 OPENCoastS, supported by atmospheric reanalyses and FES2014,  
36 complemented by the inverse barometer effect.  
37  
38  
39  
40  
41  
42  
43  
44  
45

46 The integration of hindcast simulations in OPENCoastS raises an important  
47 issue on the evaluation of the quality of those runs. A small level of in-situ data  
48 was integrated in the platform, supported by the extensive network of  
49 EMODNET physics' water level stations and by processing Sentinel images for  
50 water/land interface detection. However, much remains to be done regarding the  
51 evaluation of salinity and temperature, waves and velocities. Better exploitation  
52 of remote sensing either from satellites (for temperature, salinity and wave  
53 comparisons) or radar networks (for surface velocities) will be considered along  
54 with a more extensive usage of EMODNET data for the same variables.  
55  
56  
57  
58  
59  
60  
61  
62  
63  
64  
65

1  
2  
3  
4  
5  
6  
7  
8  
9  
10  
11  
12  
13  
14  
15  
16  
17  
18  
19  
20  
21  
22  
23  
24  
25  
26  
27  
28  
29  
30  
31  
32  
33  
34  
35  
36  
37  
38  
39  
40  
41  
42  
43  
44  
45  
46  
47  
48  
49  
50  
51  
52  
53  
54  
55  
56  
57  
58  
59  
60  
61  
62  
63  
64  
65

Finally, the current implementation of OPENCoastS in EOSC should also be improved to allow for better multisite scalability, elasticity, high availability and redundancy to guarantee services operation. The goals are to improve data movement between hosting infrastructure sites, using the EGI Data Transfer, and automation, scalability and elasticity using Infrastructure Manager and EGI Cloud Container Compute. Moreover, this approach will also provide an improved deployment of a distributed database solution, so that all available OPENCoastS infrastructure providers can be used transparently. This solution targets the guarantee of optimized and timely delivery of service which is fundamental for quality assurance of operational forecast systems and its high demand for immediate access to the computational resources.

## Acknowledgements

This work was funded by the European Commission through the H2020 projects EOSC-hub (Grant Agreement No 777536) and EOSC-Synergy (Grant Agreement No 857647), by Lisboa2020 Operational Program through the INCD project (LISBOA-01-0145-FEDER-022153) and by the Fundação para a Ciência e a Tecnologia through projects MOSAIC.pt (PTDC/CTA-AMB/28909/2017) and AQUAMON (PTDC/CCI-COM/30142/2017). This work made use of results produced with the support of the Portuguese National Grid Initiative; more information in <https://wiki.ncg.ingrid.pt>.

The test cases of Figueira da Foz Harbor were made thanks to bathymetric data made available by the Coastal Monitoring Programme of Continental Portugal - COSMO, co-funded within POSEUR-09-2015-25, and thanks to bathymetric data obtained within the project NAVSAFETY, funded by the Direção-Geral de Política do Mar, in the scope of the Fundo Azul.

## References

- Allan, J., Priest, G.R., Zhang, Y.J. and Gabel, L. (2018). Maritime tsunami evacuation guidelines for the Pacific Northwest coast of Oregon. *Natural Hazards*, 94, 21–52. <https://doi.org/10.1007/s11069-018-3372-2>
- APA – Agência Portuguesa do Ambiente (2012) *Plano de Gestão da Região Hidrográfica do Tejo, Relatório Técnico – Síntese*. Ministério da Agricultura, do Mar, do Ambiente e do Ordenamento do Território.

- 1  
2  
3  
4  
5  
6  
7  
8  
9  
10  
11  
12  
13  
14  
15  
16  
17  
18  
19  
20  
21  
22  
23  
24  
25  
26  
27  
28  
29  
30  
31  
32  
33  
34  
35  
36  
37  
38  
39  
40  
41  
42  
43  
44  
45  
46  
47  
48  
49  
50  
51  
52  
53  
54  
55  
56  
57  
58  
59  
60  
61  
62  
63  
64  
65
- Bedri, Z., A. Corkery, J.J. O'Sullivan, M.X. Alvarez, A.C. Erichsen, L.A. Deering, K. Demeter, G.M.P. O'Hare, W.G. Meijer, B. Masterson (2014). An integrated catchment-coastal modelling system for real-time water quality forecasts, *Environmental Modelling & Software*, 61, 458-476. DOI: 10.1016/j.envsoft.2014.02.006
- Bertin, X., Li, K., Roland, A., Zhang, Y. J., Breilh, J. F., & Chaumillon, E. (2014). A modeling-based analysis of the flooding associated with Xynthia, central Bay of Biscay. *Coastal Engineering*, 94, 80-89. DOI: 10.1016/j.coastaleng.2014.08.013
- Bertin, X., Li, K., Roland, A., & Bidlot, J. R. (2015). The contribution of short-waves in storm surges: Two case studies in the Bay of Biscay. *Continental Shelf Research*, 96, 1-15. DOI: 10.1016/j.csr.2015.01.005
- Brevik, O., A.A. Allen, 2008. An operational search and rescue model for the Norwegian Sea and the North Sea, *Journal of Marine Systems*, 69/1-2: 99-113. DOI: 10.1016/j.jmarsys.2007.02.010
- Brotas V., Gameiro C. (2009). Padrões de variabilidade sazonal e interanual de nutrientes e fitoplâncton no estuário do Tejo. Plano de Ordenamento do Estuário do Tejo, Saberes e Reflexões. Gabinete de Ordenamento do Território, Administração da Região Hidrográfica do Tejo, Ministério do Ambiente, do Ordenamento do Território e do Desenvolvimento Regional, 150-153.
- Castanheiro, J.M. (1986). Distribution, transport and sedimentation of suspended matter in the Tejo Estuary. In *Estuarine processes: An application to the Tagus Estuary*; Secretaria de Estado do Ambiente e Recursos Naturais: Lisboa, Portugal, pp. 75–90.
- Chen, C., Robert C. Beardsley, Richard A Luetlich Jr., Joannes J. Westerink, Harry Wang, Will Perrie, Qichun Xu, Aaron S. Donahue, Jianhua Qi, Huichan Lin, Liuzhi Zhao, Patrick C. Kerr, Yanqiu Meng, Bash Toulany (2013). Extratropical storm inundation testbed: Intermodel comparisons in Scituate, Massachusetts, *J. Geophys. Res. Oceans*, 118, 5054-5073, doi:10.1002/jgrc.20397.
- Chiu, C., Huang, C., Wu, L., Zhang, Y., Chuang, L., Fan, Y., Yu, H-C. (2018) Forecasting of oil-spill trajectories by using SCHISM and X-band radar, *Marine Pollution Bulletin*, 137, 566-581.
- Codiga, D.L. (2011). *Unified Tidal Analysis and Prediction Using the Utide Matlab Functions*. Graduate School of Oceanography, University of Rhode Island Narragansett, RI.

- 1 Du, J., Park, K., Shen, J., Zhang, Y. J., Yu, X., Ye, F., Wang, Z., Rabalais, N.  
2 N. (2019). A hydrodynamic model for Galveston Bay and the shelf in the  
3 northern Gulf of Mexico, *Ocean Sciences*, 15, 951-966,  
4 <https://doi.org/10.5194/os-15-951-2019>  
5
- 6 Elsner, J.B., K.-B. Liu (2003). Examining the ENSO-Typhoon Hypothesis,  
7 *Climate Research*. 25, 43. DOI:10.3354/cr025043  
8
- 9 Fernandez-Montblanc, T., M.I. Vousdoukas, P. Ciavola, E. Voukouvalas, L.  
10 Mentaschi, G. Breyiannis, L. Feyen, P. Salamon, (2019). Towards robust  
11 pan-European storm surge forecasting, *Ocean Modelling*, 133, 129-144,  
12 <https://doi.org/10.1016/j.ocemod.2018.12.001>.  
13
- 14 Ferrarin, C., Davolio, S., Bellafiore, D., Ghezzi, M., Maicu, F., Mc Kiver, W.,  
15 Drofa, O., Umgiesser, G., Bajo, M., De Pascalis, F., Malguzzi, P., Zaggia,  
16 L., Lorenzetti, G., Manfredi, G. (2019). Cross-scale operational  
17 oceanography in the Adriatic Sea, *Journal of Operational Oceanography*,  
18 DOI: 10.1080/1755876X.2019.1576275  
19
- 20 Fortunato, A.B; Bruneau, N.; Azevedo, A.; Araújo, M.A.V.C.; Oliveira, A.  
21 (2011). Automatic improvement of unstructured grids for coastal  
22 simulations, *Journal of Coastal Research*, Special Issue 64: 1028 – 1032.  
23
- 24 Fortunato, A.B., Oliveira, A., Rogeiro, J., Tavares da Costa, R., Gomes, J.L., Li,  
25 K., Jesus, G., Freire, P., Rilo, A., Mendes, A., Rodrigues, M., Azevedo A.  
26 (2017a). Operational forecast framework applied to extreme sea levels at  
27 regional and local scales. *Journal of Operational Oceanography*. 10(1),  
28 1-15. doi:10.1080/1755876X.2016.1255471.  
29
- 30 Fortunato, A.B., Freire, P., Bertin, X., Rodrigues, M., Ferreira, J., Liberato,  
31 M.L.R. (2017b). A numerical study of the February 15, 1941 storm in the  
32 Tagus estuary. *Continental Shelf Research*. 144, 50-64.  
33 doi:10.1016/j.csr.2017.06.023.  
34
- 35 Fortunato AB, Baptista AM, Luettich Jr. RA (1997) A three-dimensional model  
36 of tidal currents in the mouth of the Tagus Estuary. *Continental Shelf  
37 Research* 17: 1689-1714.  
38
- 39 Fortunato AB, Oliveira A, Baptista AM (1999) On the effect of tidal flats on the  
40 hydrodynamics of the Tagus estuary. *Oceanol Acta*, 22, 31-44.  
41
- 42 Gameiro, C., Brotas, V. (2010). Patterns of Phytoplankton Variability in the  
43 Tagus Estuary (Portugal), *Estuaries and Coasts* 33, 311–323  
44 <https://doi.org/10.1007/s12237-009-9194-4>.  
45
- 46 Gomes, J., E. Bagnaschi, I. Campos, M. David, L. Alves, J. Martins, J. Pina, A.  
47 López-García, P. Orviz (2018). Enabling rootless Linux Containers in  
48  
49  
50  
51  
52  
53  
54  
55  
56  
57  
58  
59  
60  
61  
62  
63  
64  
65

- 1 multi-user environments: The udocker tool, *Computer Physics*  
2 *Communications*, 232, 84-97, <https://doi.org/10.1016/j.cpc.2018.05.021>.
- 3 Guérin, T., Bertin, X., Dodet, G. (2016). A numerical scheme for coastal  
4 morphodynamic modelling on unstructured grids. *Ocean Modelling*. 104,  
5 45-53. doi:10.1016/j.ocemod.2016.04.009.
- 6  
7  
8 Guerreiro, M., Fortunato, A.B., Freire, P., Rilo, A., Taborda, R., Freitas, M.C.,  
9 Andrade, C., Silva, T., Rodrigues, M., Bertin, X., Azevedo, A. (2015).  
10 Evolution of the hydrodynamics of the Tagus estuary (Portugal) in the  
11 21st century. *Revista de Gestão Costeira Integrada*, 15, 65-80.  
12 doi:10.5894/rgci515.
- 13  
14  
15  
16 Huang, W., Ye, F., Zhang, Y., Park, K., Du, J., Moghimi, S., Myers, E., Pe'eri,  
17 S., Calzada, J.R., Yu, H.C., Nunez, K., and Liu, Z. (2021) Compounding  
18 factors for extreme flooding around Galveston Bay during Hurricane  
19 Harvey, *Ocean Modelling*, 158, 101735.
- 20  
21  
22  
23 Lavaud, L., Bertin, X., Martins, K., Arnaud, G., Bouin, M. (2020) The  
24 contribution of short-wave breaking to storm surges: The case Klaus in  
25 the Southern Bay of Biscay, *Ocean Modelling*, 156.
- 26  
27  
28 Li, X., Zhong, D., Zhang, Y., Wang, Y., Wang, Y., and Zhang, H. (2018) Wide  
29 river or narrow river: Future river training strategy for Lower Yellow  
30 River under global change, *International Journal of Sediment Research*,  
31 <https://doi.org/10.1016/j.ijsrc.2018.04.001>
- 32  
33  
34  
35 Liu, W.-C. ; Huang, W.-C., (2020). Investigating typhoon-induced storm surge  
36 and waves in the coast of Taiwan using an integrally-coupled tide-surge-  
37 wave model, *Ocean Engineering*, 107571, DOI:  
38 10.1016/j.oceaneng.2020.107571.
- 39  
40  
41 Longuet-Higgins, M.S., Stewart, R. (1964). Radiation stresses in water waves; a  
42 physical discussion, with applications. *Deep Sea Research and*  
43 *Oceanographic Abstracts*, 11/ 4. 529–562.
- 44  
45  
46 Lyard, F.H., Allain, D.J., Cancet, M., Carrère, L., Picot, N. (2020). FES2014  
47 global ocean tides atlas: design and performances, *Ocean Sciences*,  
48 <https://os.copernicus.org/preprints/os-2020-96/>.
- 49  
50  
51 Lynett, P.J., Gately, K., Wilson, R., Montoya, L., Adams, L., Arcas, D., Aytore,  
52 B., Bai, Y., Bricker, J.D., Castro, M.J., Cheung, K., David, C., Dogan, G.,  
53 Escalante, C., Gonzalez, F.I., Gonzalez-Vida, J., Grilli, S.T., Heitmann,  
54 T.W., Horrillo, J., KaÅnoÃ,,Ålu, U., Kian, R., Kirby, J.T., Li, W.,  
55 Macaas, J., Nicolsky, D.J., Ortega, S., Pampell-Manis, A., Park, Y.,  
56 Roeber, V., Sharghivand, N., Shelby, M., Shi, F., Tehranir, B., Tolkova,  
57  
58  
59  
60  
61  
62  
63  
64  
65

- 1 E., Thio, H., Velioglu, D., Yalciner, A., Yamazaki, Y., Zaytsev, A.,  
2 Zhang, Y. (2017) Inter-Model Analysis of Tsunami-Induced Coastal  
3 Currents, *Ocean Modelling*, 114, 14-32  
4
- 5 Nahon, A., Fortunato, A.B., Azevedo, A., Oliveira, F.S.B.F., Oliveira, J.N.C.,  
6 Rogeiro, J., Jesus, G., Oliveira, A., Silva P.A., and Freire, P., 2020.  
7 Implementation and validation of an operational forecasting system for  
8 nearshore hydrodynamics with OPENCoastS. *Atas das 6as Jornadas de*  
9 *Engenharia Hidrográfica / Ias Jornadas Luso-Espanholas de*  
10 *Hidrografia*. 203-206, Instituto Hidrográfico, Lisboa  
11
- 12 Neves FS (2010) *Dynamics and hydrology of the Tagus estuary: results from in*  
13 *situ observations*. PhD Thesis, Universidade de Lisboa, Portugal.  
14
- 15 Oke, Peter R., Roger Proctor, Uwe Rosebrock, Richard Brinkman, Madeleine L.  
16 Cahill, Ian Coghlan, Prasanth Divakaran, Justin Freeman, Charitha  
17 Pattiaratchi, Moninya Roughan, Paul A. Sandery, Amandine Schaeffer,  
18 and Sarath Wijeratne (2016). The Marine Virtual Laboratory (version 2.1):  
19 enabling efficient ocean model configuration, *Geosci. Model Dev.*, 9,  
20 3297–3307, 2016, <https://doi.org/10.5194/gmd-9-3297-2016>.  
21
- 22 Oliveira A, Baptista A (1997) Diagnostic modeling of residence times in  
23 estuaries. *Water Resour Res* 33: 1935-1946.  
24
- 25 Oliveira, A., J. Rogeiro, G. Jesus, A.B. Fortunato, L. David, M. Rodrigues, J.  
26 Costa, T. Mota, J.L. Gomes, R. Matos (2015). Sub-chapter 3.13 - Real-  
27 time monitoring and forecast platform to support early warning of faecal  
28 contamination in recreational waters. In *Climate Change, Water Supply*  
29 *and Sanitation: Risk Assessment, Management, Mitigation and Reduction*,  
30 102 - 112. London: IWA Publishing.  
31
- 32 Oliveira, A., Fortunato, A.B., Rogeiro, J., Teixeira, J., Azevedo, A. , Lavaud, L.,  
33 Bertin, X., Gomes, J., David, M., Pina, J., Rodrigues, M., Lopes, P. (2020).  
34 OPENCoastS: An open-access service for the automatic generation of  
35 coastal forecast systems, *Environmental Modelling & Software* 124,  
36 <https://doi.org/10.1016/j.envsoft.2019.104585>  
37
- 38 Orseau, S., Huybrechts, N., Tassi, P., Kaidi, S., Klein, F., 2021. NavTEL: Open-  
39 Source Decision Support Tool for Ship Routing and Underkeel Clearance  
40 Management in Estuarine Channels, *Journal of Waterway, Port, Coastal,*  
41 *and Ocean Engineering*, 147, 2, doi: 10.1061/(ASCE)WW.1943-  
42 5460.0000610.  
43
- 44 Roberts, K.J., Pringle, W.J., Westerink, J.J., Contreras, M.T., Wirasaet, D.  
45 (2019). On the automatic and a priori design of unstructured mesh  
46  
47  
48  
49  
50  
51  
52  
53  
54  
55  
56  
57  
58  
59  
60  
61  
62  
63  
64  
65

1 resolution for coastal ocean circulation models, *Ocean Modelling*, 144:  
2 101509.

3 Rodrigues, M., Fortunato, A.B. (2017). Assessment of a three-dimensional  
4 baroclinic circulation model of the Tagus estuary (Portugal). *AIMS*  
5 *Environmental Science*, 4(6), 763-787.  
6 doi:10.3934/environsci.2017.6.763.

7  
8  
9  
10 Rodrigues, M., Rogeiro, J., David, L., Fortunato, A.B., Oliveira, A. (2016).  
11 Análise de sensibilidade à incerteza dos forçamentos na previsão da  
12 qualidade da água em tempo real. *Atas do 13º Congresso da Água*  
13 (Lisboa, Portugal), 15pp.

14  
15  
16  
17 Rodrigues, M., Fortunato, A.B., Freire, P. (2019). Saltwater intrusion in the  
18 upper Tagus estuary during droughts. *Geosciences*, 9(9), 400. doi:  
19 10.3390/geosciences9090400

20  
21  
22 Roland, A., Zhang, Y. J., Wang, H. V., Meng, Y., Teng, Y.-C., Maderich, V.,  
23 Brovchenko, I., Dutour-Sikiric, M., Zanke, U. (2012). A fully coupled 3D  
24 wave-current interaction model on unstructured grids, *Journal of*  
25 *Geophysical Research*, 117(C11).

26  
27  
28 Stanev, E.V., Schulz-Stellenfleth, J., Staneva, J., Grayek, S., Grashorn, S.,  
29 Behrens, A., Koch, W., and Pein, J. (2016) Ocean forecasting for the  
30 German Bight: from regional to coastal scales, *Ocean Science*, 12, 1105-  
31 1136

32  
33  
34  
35 Stokes, K., Poate, T., Masselink, G., King, E., Saulter, A. and Ely, N. (2021)  
36 Forecasting coastal overtopping at engineered and naturally defended  
37 coastlines, *Coastal Engineering*, 164, 103827,  
38 <https://doi.org/10.1016/j.coastaleng.2020.103827>.

39  
40  
41 Trotta, F., Fenu, E., Pinardi, N., Bruciaferri, D., Giacomelli, L., Federico, I.,  
42 Coppini, G. (2016) A Structured and Unstructured grid Relocatable ocean  
43 platform for Forecasting (SURF), *Deep Sea Research Part II: Topical*  
44 *Studies in Oceanography*, Volume 133, Pages 54-75,  
45 <https://doi.org/10.1016/j.dsr2.2016.05.004>.

46  
47  
48  
49 Trotta F, Federico I, Pinardi N, Coppini G, Causio S, Jansen E, Iovino D and  
50 Masina S (2021) A Relocatable Ocean Modeling Platform for  
51 Downscaling to Shelf-Coastal Areas to Support Disaster Risk Reduction.  
52 *Front. Mar. Sci.* 8, 642815. doi: 10.3389/fmars.2021.642815.

53  
54  
55  
56 Turner, P., Baptista, A.M. (1993). *ACE/gredit User's Manual. Software for*  
57 *Semi-automatic Generation of Two-Dimensional Finite Element Grids.*



Center for Coastal and Land-Margin Research, Oregon Graduate Institute of Science & Technology.

- 1  
2  
3  
4  
5  
6  
7  
8  
9  
10  
11  
12  
13  
14  
15  
16  
17  
18  
19  
20  
21  
22  
23  
24  
25  
26  
27  
28  
29  
30  
31  
32  
33  
34  
35  
36  
37  
38  
39  
40  
41  
42  
43  
44  
45  
46  
47  
48  
49  
50  
51  
52  
53  
54  
55  
56  
57  
58  
59  
60  
61  
62  
63  
64  
65
- Umgiesser, G., Bajo, M., Ferrarin, C., Cucco, A., Lionello, P., Zanchettin, D., Papa, A., Tosoni, A., Ferla, M., Coraci, E., Morucci, S., Crosato, F., Bonometto, A., Valentini, A., Orlic, M., Haigh, I.D., Nielsen, J.W., Bertin, X., Fortunato, A.B., Gómez, B.P., Fanjul, A.A., Paradis, D., Jourdan, D., Pasquet, A., Murre, B., Tintoré, J., Nicholls, R.J., in press. The prediction of floods in Venice: methods, models and uncertainty, *Natural Hazards and Earth System Science*. DOI: 10.5194/nhess-2020-361
- Valente AS, Silva JCB (2009). On the observability of the fortnightly cycle of the Tagus estuary turbid plume using MODIS ocean colour images. *Journal of Marine Systems*, 75 (1-2), 131-137.
- Vaz N, Dias JM (2014). Residual currents and transport pathways in the Tagus estuary, Portugal: the role of freshwater discharge and wind, *Journal of Coastal Research*, Special Issue 70, 610-615.
- Viegas, C.N., S. Nunes, R. Fernandes, R. Neves, 2009. Streams contribution on bathing water quality after rainfall events in Costa do Estoril-a tool to implement an alert system for bathing water quality, *Journal of Coastal Research*, Special Issue 56, part 2: 1691-1695
- Wang, Z., Chai, F., Dugdale, R., Liu, Q., Xue, H., Wilkerson, F., Chao, Y., Zhang, Y., and Zhang, H. (2020) The interannual variabilities of chlorophyll and nutrients in San Francisco Bay: A modeling study. *Ocean Dynamics*. 70, 1169-1186. <https://doi.org/10.1007/s10236-020-01386-0>
- The WAVEWATCH III R Development Group (WW3DG) (2016). *User manual and system documentation of WAVEWATCH III R version 5.16*. Tech. Note 329, NOAA/NWS/NCEP/MMAB, College Park, MD, USA, 326 pp.
- Werner, M., J. Schellekens, P. Gijbers, M. van Dijke, O. van den Akker, K. Heynert, (2013). The Delft-FEWS flow forecasting system, *Environmental Modelling & Software*, 40, 65–77.
- Wolf, B., Kiel, E., Hagge, A., Krieg, H.-J., Feld, C.K. (2009). Using the salinity preferences of benthic macroinvertebrates to classify running waters in brackish marshes in Germany. *Ecological Indicators*, 9, 837-847.
- Zhang, Y., Ateljevich, E., Yu, H.-C., Wu, C.-H., Yu, J.C.S. (2015). A new vertical coordinate system for a 3D unstructured-grid model. *Ocean Modelling*, 85, 16-31. <https://doi.org/10.1016/j.ocemod.2014.10.003>

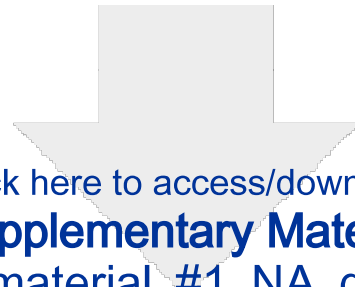
Zhang, Y.J., Ye, F., Stanev, E.V., Grashorn, S., 2016. Seamless cross-scale modeling with schism. *Ocean Modelling*, 102, 64–81.

1  
2  
3  
4  
5  
6  
7  
8  
9  
10  
11  
12  
13  
14  
15  
16  
17  
18  
19  
20  
21  
22  
23  
24  
25  
26  
27  
28  
29  
30  
31  
32  
33  
34  
35  
36  
37  
38  
39  
40  
41  
42  
43  
44  
45  
46  
47  
48  
49  
50  
51  
52  
53  
54  
55  
56  
57  
58  
59  
60  
61  
62  
63  
64  
65

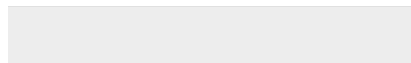
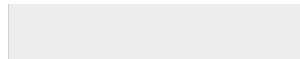
**Declaration of interests**

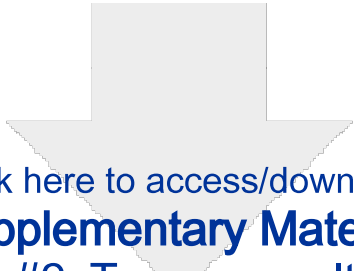
The authors declare that they have no known competing financial interests or personal relationships that could have appeared to influence the work reported in this paper.

The authors declare the following financial interests/personal relationships which may be considered as potential competing interests:



Click here to access/download  
**Supplementary Material**  
Suppl\_material\_#1\_NA\_grid.docx





[Click here to access/download](#)

**Supplementary Material**

Suppl\_material\_#2\_Tagus\_results\_stations.docx

